ERDC/GSL TR-16-33

Geotechnical and Structures Laboratory

US Army Corps
of Engineers®
Engineer Research and
Development Center

ERDC
INNOVATIVE SOLUTIONS
for a safer, better world

U.S. Air Force Airfield Damage Repair (ADR) Modernization Program

Evaluation of Flowable Fill Surface Performance

William D. Carruth and Dr. Isaac L. Howard

November 2016

The U.S. Army Engineer Research and Development Center (ERDC) solves the nation's toughest engineering and environmental challenges. ERDC develops innovative solutions in civil and military engineering, geospatial sciences, water resources, and environmental sciences for the Army, the Department of Defense, civilian agencies, and our nation's public good. Find out more at www.erdc.usace.army.mil.

To search for other technical reports published by ERDC, visit the ERDC online library at http://acwc.sdp.sirsi.net/client/default.

ERDC/GSL TR-16-33
November 2016

Evaluation of Flowable Fill Surface Performance

William D. Carruth, P.E.

Geotechnical and Structures Laboratory
U.S. Army Engineer Research and Development Center
3909 Halls Ferry Road
Vicksburg, MS 39180-6199

Isaac L. Howard, PhD, P.E.

Associate Professor, Materials and Construction Industries Chair
Mississippi State University, Civil and Environmental Engineering Department
501 Hardy Road, 235F Walker Hall, P.O. Box 9546
Mississippi State, MS 39762-9546

Final report

Prepared for Headquarters, Air Force Civil Engineer Center
Tyndall AFB, FL 32403-5319

Under "Airfield Damage Repair (ADR) Modernization Program,"
Project Number 333159

Abstract

In 2004, legacy ADR systems were found to be inadequate for supporting runway operations of large military aircraft. The inability to effectively operate both fighter and heavy cargo aircraft on the same repaired runway after an attack poses significant operational challenges. The U.S. Air Force Air Combat Command began the Airfield Damage Repair (ADR) Modernization Program to develop technologies to address operational limitations of current ADR equipment, materials, and tactics. The objective of the program was to modernize the Air Force's ADR capability through development of new solutions suitable for both fighter and cargo aircraft and scalable to the threat or damage. Scalable ADR solutions improve minimum operating strip (MOS) decision making options. Technical solutions were successfully demonstrated as a part of the Critical Runway AssessmenT and Repair (CRATR) Joint Capabilities Technology Demonstration (JCTD) Program. One of the solutions successfully demonstrated was use of rapid-setting flowable fill backfill. This report describes testing of rapid-setting flowable fill material as a surface capping material for expedient crater repairs at the Silver Flag Exercise Site on Tyndall Air Force Base, Florida. Repairs were capped with rapid-setting flowable fill over varying types and thicknesses of backfill layers. Smaller-sized repairs were loaded with a load cart simulating F-15 aircraft traffic, while larger repairs were trafficked with simulated C-17 traffic. All repairs withstood more than 500 simulated aircraft passes before reaching failure.

Contents

Figures and Tables

Figures

Tables

Preface

This study was conducted for the U.S. Air Force's (USAF) pavement evaluation teams, contingency readiness groups, base civil engineers, major command pavement engineers, Rapid Engineer Deployable Heavy Operational Repair Squadron Engineer (RED HORSE) squadrons, and Prime Base Engineer Emergency Force (BEEF) units. Additional users of this report include Army, Navy, and Marine Corps units charged with the repair and sustainment of bomb-damaged airfield pavements.

The project described in this report is part of the USAF's Civil Engineer Modernization Program sponsored by the Headquarters, Air Force Civil Engineer Center (AFCEC), at Tyndall AFB. The Technical Monitor for this project was Dr. Craig Rutland of the AFCEC. The U.S. Army Engineer Research and Development Center (ERDC) technical manager for this project was Jeb S. Tingle, Engineer Systems and Materials Division, Geotechnical and Structures Laboratory.

At the time of publication, Dr. Timothy W. Rushing was Branch Chief, CEERD-GMA; Dr. Gordon W. McMahon was Division Chief, CEERD-ESMD; and Nicholas Boone, CEERD-GVT, was the Technical Director for Force Projection and Maneuver Support. The Deputy Director of the GSL was Dr. William P. Grogan, CEERD-GSL, and the Director was Bartley P. Durst, CEERD-GSL.

COL Bryan S. Green was the Commander of ERDC, and Dr. Jeffery P. Holland was the Director.

Unit Conversion Factors

Multiply	By	To Obtain
cubic feet	0.02831685	cubic meters
cubic yards	0.7645549	cubic meters
degrees Fahrenheit	(F-32)/1.8	degrees Celsius
feet	0.3048	meters
gallons (US liquid)	3.785412 E-03	cubic meters
inches	0.0254	meters
mils	0.0254	millimeters
pounds (force)	4.448222	newtons
pounds (force) per square inch	6.894757	kilopascals
pounds (mass)	0.45359237	kilograms
pounds (mass) per cubic foot	16.01846	kilograms per cubic meter
square feet	0.09290304	square meters
tons (2,000 pounds, mass)	907.1847	kilograms
yards	0.9144	meters

1 Introduction

1.1 Background

The U.S. Air Force Air Combat Command began the Airfield Damage Repair (ADR) Modernization Program to develop technologies to address operational limitations of current ADR equipment, materials, and tactics. The overall objective of the program is to modernize the Air Force's ADR capability through development of new ADR solutions that are suitable for fighter and cargo aircraft while scalable to the threat or damage. Since 2006, researchers at the U.S. Army Engineer Research and Development Center (ERDC) have been conducting research under the program to develop new, expedient pavement repair techniques in an effort to update repair guidance for military airfields. Damaged airfield pavements must be repaired quickly using suitable materials to reduce the total time that the airfield is removed from service, as well as to reduce the need to conduct subsequent repairs to maintain an operable pavement surface, particularly during wartime scenarios. A more complete overview of the ADR modernization program from 2006 forward can be found in Carruth et al. (2015).

Cementitious, rapid-setting concrete repair materials have been successfully demonstrated for repairing bomb-damaged concrete pavements as a part of the ADR Modernization Program. Based on results from numerous full-scale experiments, Rapid Set Concrete Mix® was identified as a versatile repair material and has been used to conduct many repairs capable of withstanding simulated and live aircraft maneuvers (C-17 and F-15E) (Priddy et al. 2013). As a result, Rapid Set Concrete Mix® is currently recommended as the surface capping material for a variety of repair types within the ADR scenario.

Rapid-setting flowable fill was first evaluated as a backfill material for crater repair in 2009 (Priddy et al. 2013). Utility Fill 1-Step 750® is a rapid-setting flowable fill material that has been selected for use as a rapid backfill alternative, because it can be easily placed with or without the use of external mixing. In cases where the rapid-setting concrete supply is limited, it could be advantageous to use rapid-setting flowable fill as a capping material in place of rapid-setting concrete, particularly in lower traffic areas. The testing described in this report was conducted to characterize the

performance of rapid-setting flowable fill as a surface capping material and to make recommendations for its use in future ADR operations.

1.2 Objective and scope

The objective of the testing described in this report was to evaluate the suitability of rapid-setting flowable fill (traditionally used as a backfill) as a capping material for expedient crater repairs. The evaluation was conducted to determine the amount of fighter and cargo aircraft operations that can be conducted on repairs capped with rapid-setting flowable fill. To achieve the objective, multiple full-scale crater repairs were conducted using rapid-setting flowable fill as the surface capping material over varying backfill types and thicknesses. Repairs were trafficked with simulated aircraft traffic, and the appropriate data were collected and analyzed in order to develop conclusions and recommendations.

The scope of this report affects activities associated with establishing and maintaining the minimum operating strip (MOS). ADR technologies improve MOS options, and as such these two items are often inter-connected. For example, if a large area of pavement exists with several discrete areas to repair, there may be an opportunity to optimize repair quality, as it is unlikely that each repair will receive equal traffic. In these cases, marginal materials might be suitable for some repairs, intermediate materials for other patches, and premium materials for most critical repairs. This report focuses more on ADR repair performance than MOS decision making, while the findings from this report can aid in MOS decision making.

1.3 Outline of chapters

Chapter 1 provides background information covering the history of the ADR program and the specific objectives and scope of the work covered in this report. Chapter 2 presents a description of the test site and describes all equipment and materials used during testing. Chapter 3 discusses the test matrix and the various types of data collected for each crater repair. Chapter 4 provides test results and analysis, while conclusions and recommendations are presented in Chapter 5. References used in preparing this report are also provided.

2 Test Site, Equipment, and Materials Description

2.1 Test site description

Flowable fill surface performance testing took place in May 2015 at the Silver Flag Exercise Site on Tyndall AFB, Florida. The test site was selected, because it is a training airfield with adequate PCC pavement thickness to support simulated aircraft traffic. The PCC thickness varied within the test area between 9 and 12 in., and the existing slabs were 15 ft by 15 ft. The site had a humid, temperate climate and the subgrade was a sand or silty-sand with a relatively high water table.

2.2 Equipment

2.2.1 Caterpillar 279C compact track loader

A Caterpillar 279C compact track loader (CTL), or skid steer, is a high-flow, rubber-tracked machine with quick-disconnect fittings that are used extensively in the modernized ADR process. The quick disconnect allows attachments to be switched out rapidly without the use of tools. Specifications for the machine can be found in Table 1.

For the ADR mission, the track loader is a multi-purpose machine that is employed for rapidly cutting around the upheaval using the wheel saw attachment, removing debris using the bucket attachment, or cleaning up with the broom attachment. The 279C CTL with the wheel saw attachment is shown in Figure 1.

Table 1. Caterpillar 279C CTL specifications.

Net power	82 hp
Operating weight	9,495 lb
Rated operating capacity	3,200 lb at 50% tipping load
Travel speed	5.0 mph
Tipping load	6,483 lb
Breakout force, tilt cylinder	7,308 lb
Maximum loader hydraulic pressure[a]	4,061 psi
Maximum loader hydraulic flow[a]	33 gal/min

[a]For high flow XPS models

Figure 1. Tracked Caterpillar 279C CTL with SW45 wheel saw attachment.

2.2.2 Caterpillar SW45 wheel saw attachment

The CTL used for testing was equipped to operate the Caterpillar SW45 wheel saw attachment as shown in Figure 1. The SW45 produces a 3.5-in.-wide cut with a maximum depth of 18 in. Specifications for the SW45 can be found in Table 2.

Table 2. SW45 wheel saw specifications.

Specification	Value
Overall width	71 in.
Overall height	57 in.
Length	78 in.
Weight	2,295 lb
Wheel width	3.5 in.
Required hydraulic flow range	24-42 gpm
Optimal hydraulic pressure range	2,611 to 4,351 psi
Wheel torque at maximum pressure	4,944 lb•ft
Wheel speed at maximum flow	115 rpm
Number of teeth	64 per wheel
Maximum depth of cut	18 in.
Sideshift travel	26 in.

2.2.3 Bucket and broom attachments

Caterpillar Bucket and BA18 broom attachments (Figure 2) for the Caterpillar 279C CTLs were used for debris removal and cleanup before, during, and/or after each crater repair test.

Figure 2. Bucket (left) and broom (right) attachments for Caterpillar 279C terrain loader.

2.2.4 Wheeled excavator

Wheeled excavators are preferred over tracked excavators for crater repair purposes, because they are more mobile and do not cause damage to the airfield pavement. The Volvo EW180C wheeled excavator was used during testing for breaking and excavation (Figure 3). Specifications for the Volvo EW180C and Volvo HB1400 hammer attachment are listed in Table 3 and Table 4, respectively. The excavator was equipped with quick-disconnect fittings for the hammer and bucket work tool attachments. The bucket used for excavation was 36 in. wide and had 8-in.-long teeth.

Figure 3. Volvo EW180C excavator with HB1400 hammer.

Table 3. Volvo EW 180C specifications.

Specification	Value
Net power	152 hp
Maximum torque	538 lb•ft at 1,400 rpm
Breakout force	24,998 lbf
Maximum digging reach	31.8 ft
Maximum digging depth	20.8 ft
Maximum travel speed	22 mph
Operating weight	36,200 to 40,600 lb

Table 4. Volvo HB 1400 specifications.

Specification	Value
Impact energy	2,500 lb•ft
Operating weight	2,932 lb
Tool diameter	4.92 in.
Acceptable oil flows	32 to 45 gpm
Oil pressure	1,958 to 2,103 psi
Impact rate	450 to 800 blows per min
Excavator weight limits	39,683 to 57,320 lb

2.2.5 Rammer-style compactor

A small rammer-style compactor was used to compact the natural subgrade, sand backfill, and crushed stone backfill material during testing. The compactor used was a Multiquip Mikasa MTX-70 (Figure 4), which has a 2.8-hp motor capable of providing 3,350 lbf of impact force. Additional specifications are displayed in Table 5. The small rammer-style compactor was used, since larger compaction equipment would be difficult to maneuver inside small craters. In addition, the smaller rammer-style compactor eliminates the logistical burden of deploying larger compaction equipment.

Figure 4. Multiquip Mikasa MTX-70 rammer-style comptactor.

Table 5. Multiquip Mikasa MTX-70 specifications.

Specification	Value
Operating Weight	165 lb
Blows per min.	690
Impact Force	3,350 lbf
Shoe jump height	3.1 in.
Shoe dimensions	13.4 in. by 11.2 in.
Engine Make/Model	Honda GX100
Engine Power	2.8 HP

2.2.6 Extendable-boom forklift

An extendable-boom forklift was used to move the 3,000-lb supersacks of pre-blended flowable fill materials. The extendable boom was a Caterpillar TL642 telescopic forklift, which was capable of lifting 6,500 lb and extending 30 ft. The extendable boom is needed so that the large super-sacks of flowable fill can be loaded into the simplified volumetric concrete mixer, as shown in Figure 5.

Figure 5. Extendable-boom forklift loading supersack into volumetric mixer.

2.2.7 Simplified volumetric concrete mixer

A specially designed tow-behind simplified volumetric concrete mixer (Figure 6) was previously designed by CemenTech Inc. in consultation with the ERDC for use in the ADR modernization program. The simplified volumetric mixer is pre-calibrated for rapid-setting cementitious repair materials to include flowable fill and concrete capping material.

The mixer is towed with a vehicle capable of pulling at least 20 tons. For the testing described in this report, the mixer was towed by a standard 12-ton dump truck. The mixer consists of a single dry-material hopper with a capacity of approximately 6 yd^3, a conveyor belt feed system, a

positive displacement water pump to meter mix water according to a fixed pump speed, two 200-gal water tanks on each side of the mixer, a washout tank with pressure washer, and a replaceable mixing auger mounted in a discharge boom at the rear of the machine. The machine is outfitted with two retractable catwalk platforms, a bin entry platform, a replacement auger, and two super sack piercing points. The only means of controlling the water-cement (w/c) ratio is by adjusting a strike-off gate, which can change the height of the dry material on the conveyor belt feeding the mix auger. Allowing more dry material to enter the mix auger results in a mix with a lower w/c ratio. The wheel for adjusting the gate height has a scale from 1 to 12, where 1 allows the least amount of material to enter the mix auger and 12 allows the most. However, typical strike-off gate settings used during production of rapid-setting flowable fill or rapid-setting concrete range from 4 to 8.

Figure 6. Simplified volumetric mixer.

2.2.8 Water truck

A commercial water truck with a 3,000-gal capacity was used for adding water to the volumetric mixer's saddle tanks and for cleanup. A 2-in.-diameter hose with a cam-lock connection was used to carry out the

process. The water truck was equipped with a power takeoff (PTO), or a powered pump that runs off the vehicle drive system.

2.3 Materials

2.3.1 Natural subgrade

The in-situ subgrade material was sampled and tested to determine its classification according to Unified Soil Classification System (USCS) per ASTM D 2487. The material classified as a gray-colored silty-sand (SM) with 2.2 percent gravel, 90.8 percent sand, and 7.0 percent fines. The fines contained in the subgrade were non-plastic.

2.3.2 Crushed limestone backfill

Crushed limestone (Figure 7) purchased from a local vendor was used as a backfill material for some test craters. Crushed limestone was selected because it can be available on some U.S. Air Force (USAF) airfields that have access to higher quality materials. The maximum aggregate size of the material was approximately 1 in. The USCS classification of the material was a well-graded gravel with silt and sand (GW-GM). The fines within the crushed limestone were non-plastic.

Figure 7. Crushed stone limestone backfill.

2.3.3 Masonry sand backfill

Commercial masonry sand (Figure 8) purchased from a local vendor was used to backfill some test craters. This material was selected to use as a backfill because it can be available in remote areas where higher quality materials are unavailable. The USCS classification of the material was a poorly graded sand (SP) with 0.5% fines. The small amount of fines observed were non-plastic.

Figure 8. Masonry sand backfill.

2.3.4 Rapid-setting flowable fill

In general, traditional flowable fill is a low-viscosity, grout-like, cementitious blend commonly composed of portland cement, fine aggregate, and water. Other materials such as fly ash, slag, foundry sand, bottom ash, and chemical admixtures are also employed in flowable fill blends. Flowable fills can be designed for traditional and rapid set times, depending upon the type and amount of cementitious materials and chemical admixtures used. The material is self-leveling, self-compacting, and flows under gravity to fill the desired volume.

Material properties established to accommodate rapid ADR include an unconfined compressive strength of 250 psi after 30 min of cure, 750 psi after 3 hr of cure, being optimally flowable as indicated by 8 to 12 in. of

flow consistency as per ASTM D6103, and exhibiting minimal shrinkage and subsidence potential. Utility Fill 1-Step 750® is a rapid-setting flowable fill material that has been selected for rapid ADR operations as discussed previously in Chapter 1 of this report. The material differs from traditional flowable fill in that it contains calcium sulfoaluminate (CSA) cement, which provides faster set times. Approximately 10% by weight of 0.25 in. size aggregate is added, since it has been shown that the abrasive characteristics make cleaning of the mix auger easier by helping remove any mixed flowable fill material that is left behind.

Flowable fill is traditionally placed using a standard transit truck or the simplified volumetric mixer. This technique is referred to as the "wet method" and uniformly distributes moisture resulting in optimal flowability and achievement of ultimate compressive strength. The Utility Fill 1-Step 750® can also be placed by the "dry method." The dry method is an expedient placement technique, where the pre-blended dry material is dispensed directly into the excavation, alleviating the requirement for a dedicated mixer. Following the placement of thin lifts of dry material (4 to 6 in.), water is metered onto the surface and allowed to percolate through the dry material. Placement using the dry method sacrifices some of the beneficial properties of flowable fill including its self-leveling behavior and up to 30% of the compressive strength. However, the material can be placed expediently without the use of additional equipment and provides sufficient bearing capacity for heavy aircraft pavement applications. The dry method is typically used when flowable fill is used as a base material beneath a rapid-setting concrete cap as described in Edwards et al. 2013, Bell et al. 2013, and Carruth et al. 2015. The volumetric mixer was used to place the flowable fill per the "wet method" for all testing described in this report since the material was being evaluated as a surface capping material.

2.3.5 Water source

The water source used to mix the rapid-setting flowable fill material was well water from the Silver Flag Exercise Site. Lovingood et al. (2015) analyzed this non-potable water source by ion chromatography and found that it contained ion concentrations (all units ppm) of 12.9 for Na^{+}, 1.2 for K^{+}, 9.8 for Mg^{2+}, 3.2 for Ca^{2+}, 0.4 for Sr^{2+}, 3.2 for F^{-}, 13.9 for Cl^{-}, 1.7 for Br^{-}, and 12.9 for SO_4^{2-}. Use of the Silver Flag well water with Utility Fill One Step 750® showed no significant effects on set time or compressive strengths tested at 0.5, 1, 2, 4, 8, 24, and 168 hr in the laboratory. The water source also did not appear to affect the general behavior of the rapid-setting flowable fill during the full-scale testing described in this report.

3 Repair Procedures

The procedure used to conduct the crater repairs described in this report was intended to match the standard crater repair process within the ADR base recovery scenario with the exception of using rapid-setting flowable fill as a capping material in place of rapid-setting concrete. The following sections describe each step in the crater repair process. The pertinent details of each repair and the overall test matrix are discussed in the next chapter.

3.1 Marking, saw cutting, breaking, and excavation processes

The standard ADR processes of marking, saw cutting, breaking, and excavation were carried out as described in previous ADR reports (Edwards et al. 2013, Bell et al. 2013, and Carruth et al. 2015). These processes were not timed, since the work was not performed by airmen nor were the appropriate amount of personnel used for the various crater repair teams (marking, saw-cutting, breaking, excavation, backfill, and capping teams). However, capping times were recorded and compared to previously established times to provide an overall assessment. This assessment is discussed in detail in Section 4.2 of this report.

For marking, the target size of the finished crater repair (8.5 ft by 8.5 ft or 15 ft by 15 ft) was measured and marked with a string line and marking paint. Since no upheaval was present, stanchions were not used in the marking process. Saw cutting was conducted using the CTL with a wheel saw attachment. For breaking and excavating, a Volvo EWC-30 wheeled excavator with the appropriate attachment (hammer or bucket) was used. A small mini-excavator was also used in some instances to remove material along the walls of the excavation. In an actual crater repair scenario, this type of fine excavation would not be conducted. However, since the thicknesses of each layer of the crater repair structure was important to the objective of the project, a tolerance of +/- 0.5 in. was imposed. Figure 9, Figure 10, and Figure 11 show the saw-cutting, breaking, and excavating processes, respectively. Figure 12 shows an excavated 8.5-ft by 8.5-ft crater, and Figure 13 displays an excavated 15-ft by 15-ft crater.

Figure 9. Saw cutting with CTL and wheel saw attachment.

Figure 10. Breaking using Volvo HB 1400 breaker attacment.

Figure 11. Excavation using the Volvo EW 180C wheeled excavator.

Figure 12. Excavated 8.5-ft by 8.5-ft crater

Figure 13. Excavated 15-ft by 15-ft crater.

3.2 Backfill process

Once excavation of the crater repairs was complete, the natural subgrade was compacted with a rammer-style compactor as shown in Figure 14. Two coverages were performed during compaction. For some craters, no backfill layer was used, and flowable fill material was placed over the subgrade as described in Section 3.4. Some craters were backfilled with either masonry sand or crushed stone. The sand and crushed stone are described in Section 2.3.

Backfill materials were placed in two separate lifts, each one approximately half of the total target thickness, with a maximum lift thickness of 6 in. The CTL and hand tools were used to place and level the material. Two coverages of compaction with the rammer-style compactor were applied, and any remaining areas of loose material were also compacted. A small amount of water was added to the masonry sand to aid compaction. Figure 15 shows compaction of the crushed stone backfill material.

Figure 14. Compaction of natural subgrade.

Figure 15. Compaction of crushed stone backfill material.

3.3 Capping process

To begin the capping process, the simplified volumetric mixer was prepared for standard operation. Six supersacks were loaded into the dry material bin, the mix water and washout tanks were filled, and the mix auger and concrete tools were sprayed with concrete release agent. The water pump gear controls were set to flowable fill. The simplified volumetric mixer is factory calibrated to provide the optimum amount of water for flowable fill (approximately 70 gal per supersack at a gate setting of 6).

During the test, the rapid-setting flowable fill supersacks were continuously loaded into the volumetric mixer, and the mix water tanks were refilled as needed. No chemical additives of any kind were used during testing, since additives are not typically used when rapid-setting flowable fill is used as a backfill in the crater repair process. Figure 16 shows placement of rapid-setting flowable fill during a large crater repair. As shown, one extension chute was used for large crater repairs. Instead of moving the tow vehicle forward and backward to placement material in different areas of the repair, the extension chute was extended or retracted as needed. Once enough material was placed into the excavation, the crater repair cap was struck off with a magnesium screed bar (Figure 17). A 12-ft-long and 20-ft-long screed bar was used for the small and large craters, respectively. While the material was still workable, the surface was screeded multiple times, particularly for

the small craters, to ensure the surface was as smooth as possible and matched the elevation of the surrounding pavement. Flat shovels and steel trowels were used to clean the edges of the repair.

Figure 16. Rapid-setting flowable fill placement during a large crater repair.

Figure 17. Screeding of rapid-setting flowable fill cap.

As discussed in Section 2.2.7, the simplified volumetric mixer has an adjustable strike off gate, allowing for small adjustments to the amount of dry material that flows into the mix auger, which adjusts the w/c ratio for

the material being placed. A gate setting of 6 is typically used when placing the rapid-setting flowable fill as backfill under craters capped with asphalt during the ADR base recovery scenario. The gate setting was changed several times during testing to determine the optimum gate setting for using flowable fill as a capping material. For small craters, a higher gate setting (larger opening) was used to place a more viscous material to improve the compressive strength. For the large crater repairs, a lower gate setting (smaller opening) was required, resulting in a more fluid material that provided more working time and an easier screeding process.

For Craters 1, 2, and 3, the gate setting was set to 6 at the beginning of the capping process, but changed to 8 for the last 6 in. of cap placement in an attempt to place a more viscous, stronger material for the surface of the repair. For Craters, 4, 5, and 6, a gate setting of 7 was used throughout the entire placement. For Crater 7, a gate setting of 7 was used at the start of the capping process, but was quickly decreased to 6 due to insufficient working time that was associated with a larger repair volume. For Crater 8, a gate setting of 6 was used at the start of the repair, but the setting was decreased to 5.5 for the top 4 in. to further increase workability. A gate setting of between 5.5 and 6 is believed to be the highest gate setting that can be used to cap a 15-ft by 15-ft crater due to the increased workability that is needed. However, when a more fluid material is placed, it is more difficult to build up material on one side of the crater during screeding. Moreover, some isolated areas of weaker material were observed during trafficking that were likely a result of the more fluid, and therefore weaker, material that was placed during larger crater repairs. The effect of the gate setting on various test results is further discussed throughout Chapter 4.

4 Test Results and Discussion

Eight crater repairs were conducted in support of the research effort documented in this report. Key variables for testing rapid-setting flowable fill for use as a surface capping material were crater size, base material, base thickness, surface cap thickness, and aircraft type. Table 6 displays the crater repair test matrix used during testing and lists the value for each key variable. The crater numbers are referenced throughout the remainder of the report.

Table 6. Overall test matrix.

Crater No.	Aircraft Traffic	Crater Size (ft by ft)	Backfill or Base Material	Base Target Thickness (in.)	[a]FF Cap Target Thickness (in.)
1	F-15	8.5 by 8.5	None	N/A	20
2	F-15	8.5 by 8.5	None	N/A	22
3	F-15	8.5 by 8.5	None	N/A	24
4	F-15	8.5 by 8.5	Sand	12	12
5	F-15	8.5 by 8.5	Crushed Stone	10	12
6	F-15	8.5 by 8.5	Crushed Stone	12	12
7	C-17	15 by 15	None	N/A	24
8	C-17	15 by 15	Crushed Stone	12	12

[a]FF refers to flowable fill.

4.1 Weather conditions

Craters 1, 2, and 3 were repaired on 15 May 2015, Craters 4, 5, and 6 on 17 May 2015, Crater 7 on 19 May 2015, and Crater 8 on 20 May 2015. Table 7 gives the air temperature, humidity, and weather conditions during crater repair activities. As shown, in general, the weather conditions during testing consisted of an air temperature in the mid 80s°F, humidity around 70%, and dry conditions.

Table 7. Weather conditions during crater repairs.

Date	Activity	Time	Air Temperature (°F)	Humidity (%)	Conditions
Craters 1, 2, and 3					
5/15/15	Placement	1100	84	64	Mostly Cloudy
	Placement	1200	85	65	Scattered Clouds
	Placement	1300	85	66	Scattered Clouds
	Curing	1400	85	68	Mostly Cloudy
	Curing	1500	85	68	Mostly Cloudy
	Trafficking	1600	85	65	Mostly Cloudy
	Data Collection	1700	80	73	Mostly Cloudy
Craters 4, 5, and 6					
5/17/15	Placement	0900	81	78	Partly Cloudy
	Placement	1000	82	70	Scattered Clouds
	Placement	1100	86	62	Clear
	Curing	1200	86	68	Clear
	Curing	1300	86	65	Clear
	Trafficking	1400	85	70	Scattered Clouds
	Data Collection	1500	86	70	Mostly Cloudy
Crater 7					
5/19/15	Placement	1100	85	66	Clear
	Placement	1200	85	63	Partly Cloudy
	Curing	1300	86	61	Partly Cloudy
	Curing	1400	85	68	Clear
	Trafficking	1500	85	67	Partly Cloudy
	Trafficking	1600	85	67	Partly Cloudy
	Data Collection	1700	84	68	Clear
Crater 8					
5/20/15	Placement	1100	84	74	Scattered Clouds
	Curing	1200	86	70	Scattered Clouds
	Curing	1300	86	68	Partly Cloudy
	Trafficking	1400	86	70	Partly Cloudy
	Trafficking	1500	86	70	Clear
	Trafficking	1600	86	70	Clear
	Data Collection	1700	85	72	Clear

Source: www.wunderground.com; Tyndall AFB, FL

4.2 Repair capping times

Although the repairs described in this report were performed by three ERDC technicians and not five enlisted airmen (typical capping team size), the capping times were recorded for each crater to loosely compare the times to those listed in the interim USAF ADR tactics, techniques, and procedures (TTPs). Other repair activities such as saw-cutting, breaking, excavating, and backfilling were not recorded at all, but expected times for these repair activities are well-established and documented in the interim ADR TTPs.

Table 8 displays the time to cap each crater and the total thickness of rapid-setting flowable fill. For Craters 1, 2, and 3, the rapid-setting flowable fill essentially acts as the backfill and cap in one layer but is referred to as a cap for consistency. For an 8.5-ft by 8.5-ft crater repair with a thickness of 24 in., the interim ADR TTPs allow 11 min for backfill and 11 min for capping.

Table 8. Rapid-setting flowable fill capping times.

Crater No.	Aircraft Traffic	Crater Size (ft by ft)	Cap Target Thickness (in)	Capping Time (min.)
1	F-15	8.5 by 8.5	20	22
2	F-15	8.5 by 8.5	22	22
3	F-15	8.5 by 8.5	24	31
4	F-15	8.5 by 8.5	12	13
5	F-15	8.5 by 8.5	12	12
6	F-15	8.5 by 8.5	12	14
7	C-17	15 by 15	24	77
8	C-17	15 by 15	12	49

For Crater 3, a 24-in.-thick repair was performed in 31 min, which is somewhat higher than the 22 min that the draft TTPs allow for backfilling and capping a crater of the same size. Crater 3 was the first crater repair conducted, and experience allowed capping times to improve to 22 min for Craters 1 and 2 at slightly reduced thicknesses. For Craters 4, 5, and 6, the capping times were all close to the 11-min target, and the target thickness for Craters 4 to 6 was greater than the target of 10 in. that is discussed in the TTPs. Carruth et al. (2015) reported that the average time to place one 15-ft by 15-ft, 12-in.-thick section of a crater cap was 33.5 min. Crater 7 took 51 min to cap, but the reduction in personnel likely caused an

increase in time needed to place the cap. It is recommended that capping times for rapid-setting flowable fill be established in future ADR demonstrations that utilize troop construction.

4.3 Subgrade and backfill test results

Table 9 provides classification and gradation results for the subgrade, sand fill material, and crushed limestone. The natural subgrade had considerably more particles passing the No. 40 sieve than the masonry sand, and also had more fines, which was reflected in the lower fineness modulus. The masonry sand had a fineness modulus just below the range of typical values used in ready-mixed concrete (2.3 to 3.1). The crushed limestone was a fairly traditional gradation for a crushed stone base material.

Table 9. Subrade and backfill gradation results.

Material	Natural Subgrade	Masonry Sand	Crushed Limestone
Identification	NS	MS	LS
Classification	Silty Sand (SM), Gray	Sand (SP), Brown	Gravel (GW-GM) with Silt & Sand, Gray
% Finer 25.4 mm	99.3	100	86.7
% Finer 12.7 mm	98.7	100	62.3
% Finer No. 4	97.8	100	43.9
% Finer No. 10	97.4	98.4	32.2
% Finer No. 40	93.7	45.0	19.6
% Finer No. 200	7.0	0.5	9.1
% Gravel	2.2	0.0	56.1
% Sand	90.8	99.5	34.8
% Silt	3.2	$\leq$ 0.5	6.8
% Clay	3.8	$\leq$ 0.5	2.3
Fineness Modulus	1.13	2.14	5.13
C_u	1.79	3.05	129.11
C_c	1.11	0.95	2.38
D_{50}	0.20	0.47	6.46

Table 10 summarizes all density and moisture data collected with a nuclear gauge per ASTM C2922 and D3017. Proctor compaction was not performed for these materials, so quantifiable comparisons between craters for subgrade densities is not advised since there may be material differences explaining some of the densities reported. In an overall sense, subgrade density dropped 0.7 pcf per percent of added moisture, but the R^2 for the

linear regression was only 0.22. Subgrade density varied from 101.0 pcf to 113.6 pcf (12.6 pcf range), while subgrade moisture content varied from 8.0 to 14.6% (6.6% range). Craters 4, 5, and 6 showed considerably more within crater subgrade density variability (range of 4.7 to 7.7 pcf within a given crater) than the other craters (0.8 to 2.9 pcf within a given crater).

Table 10. Subrade and backfill nuclear density test results.

Crater	Material	Dry Density (pcf)			Moisture Content (%)		
		Results	Avg.	Range	Results	Avg.	Range
1	Subgrade	101.8, 102.9, 104.7	103.1	2.9	9.5, 7.0, 7.6	8.0	2.5
2	Subgrade	107.7, 108.6, 106.2	107.5	2.4	8.0, 7.5, 8.6	8.0	1.1
3	Subgrade	112.6, 113.4, 114.7	113.6	2.1	8.7, 9.0, 8.3	8.6	0.7
4	Subgrade	98.7, 103.8, 100.6	101.0	5.1	14.2, 12.5, 15.3	14.0	2.8
4	Sand Backfill	104.7, 105.6, 103.5	104.6	2.1	2.9, 2.7, 2.8	2.8	0.2
5	Subgrade	105.0, 112.5, 104.8	107.4	7.7	11.1, 8.5, 9.1	9.6	2.6
5	Crushed Stone Backfill	139.9, 138.2, 139.0	139.0	1.7	3.1, 2.7, 2.7	2.8	0.4
6	Subgrade	109.6, 112.0, 107.1	109.6	4.9	9.3, 7.9, 10.3	9.2	2.4
6	Crushed Stone Backfill	137.4, 138.8, 136.5	137.6	2.3	3.1, 2.9, 2.6	2.9	0.5
7	Subgrade	105.2, 104.1, 105.1	104.8	1.1	11.7, 12.0, 11.8	11.8	0.3
8	Subgrade	105.9, 106.5, 106.7	106.4	0.8	13.1, 17.7, 13.0	14.6	4.7
8	Crushed Stone Backfill	134.6, 127.6, 131.2	131.1	7.0	3.5, 2.8, 2.6	3.0	0.9

Comparison between limestone backfill densities is reasonable, since the material was taken from the same source. Craters 5, 6, and 8 utilized limestone backfill (classified as GW-GM). All three craters had essentially the same moisture content (2.8 to 3.0%), whereas Craters 5 and 6 were considerably more dense (137.9 to 139.0 pcf) than Crater 8 (131.1 pf). Variability of Crater 8's backfill compaction was also noticeably higher than Craters 5 and 6 (range of 7.0 pcf versus 2.0 pcf on average). Performance of Crater 8 should be interpreted in the context that the backfill did not appear as well compacted as the other limestone backfill sections.

Dynamic cone penetrometer (DCP) test results are provided in Table 11. DCP efforts followed ASTM D6951. A 17.6-lb hammer was used for all testing, and DCP penetration versus blow count data was converted to California Bearing Ratio (CBR) values with equation 1 of D6951

throughout this effort. DCP and density readings were arbitrary with respect to each other in terms of locations evaluated.

The average subgrade CBRs for Craters 1, 2, and 3 were very similar. Subgrade CBRs for Craters 4, 5, 6, were also similar to each other and much higher than Craters 1, 2, and 3. The additional confinement of the overlying backfill could explain the increased CBR for Craters 4, 5, and 6. The SP backfill used for Crater 4 had very low CBR values for a backfill, and based on DCP measurements, provided the lowest overall CBR support of any of the eight craters. The average Crater 4 CBR was 6 percent, which was lower than any of the natural subgrade CBR values. Craters 5 and 6 were practically the same with a CBR of around 50 percent, whereas Crater 8 had a CBR around half that of Craters 5 and 6. Table 10 points to the most likely reason for this difference being that the Crater 8 backfill was compacted to a dry density around 7 pcf less than the other two craters at essentially the same moisture content. With regard to the natural subgrade, Craters 5 and 6 were again practically the same, with an average CBR just over 30. Overall, Crater 8's backfill and natural subgrade support needs to be considered when interpreting performance results presented elsewhere in this report.

Table 11. CBR test results calculated from DCP measurements.

Crater	Test No.	Subgrade Avg. CBR (%)	Backfill Thickness (in)	Material	Avg. CBR (%)
1	1	14	0	None	---
1	2	15	0	None	---
1	3	15	0	None	---
1	*Avg*	*15*	*0*	*None*	*—*
2	1	15	0	None	---
2	2	14	0	None	---
2	3	14	0	None	---
2	***Avg***	***14***	***0***	***None***	***—***
3	1	11	0	None	---
3	2	14	0	None	---
3	3	15	0	None	---
3	*Avg*	*13*	*0*	*None*	---
4	**1**	**22**	**12**	**Sand**	**3**
4	2	27	12	Sand	4
4	3	27	12	Sand	4

Crater	Test No.	Subgrade	Backfill		
		Avg. CBR (%)	Thickness (in)	Material	Avg. CBR (%)
4	*Avg*	*25*	*12*	*Sand*	*4*
5	1	33	10	Crushed Stone	45
5	2	29	10	Crushed Stone	47
5	3	32	10	Crushed Stone	56
5	*Avg*	*31*	*10*	*Crushed Stone*	*49*
6	1	29	12	Crushed Stone	51
6	2	31	12	Crushed Stone	47
6	3	38	12	Crushed Stone	53
6	*Avg*	*33*	*12*	*Crushed Stone*	*50*
7	1	19	0	None	---
7	2	25	0	None	---
7	3	24	0	None	---
7	*Avg*	*23*	*0*	*None*	*—*
8	1	45	12	Crushed Stone	24
8	2	42	12	Crushed Stone	22
8	3	41	12	Crushed Stone	26
8	*Avg*	*43*	*12*	*Crushed Stone*	*24*

4.4 Load cart trafficking test results

4.4.1 Description of load carts and traffic patterns

Trafficking of each repair was conducted using a simulated F-15E (Craters 1 through 6) or C-17 (Craters 7 and 8) aircraft load. The single-wheel F-15E load cart was loaded to 35,235 lb and a 325-psi tire pressure (Figure 18). The F-15 traffic pattern was an approximate normal distribution as shown in (Figure 19). A multiple-wheel C-17 load cart was used to simulate one-half of the main gear of a C-17 fully loaded to its maximum take-off weight of approximately 586,000 lb. The multiple-wheel C-17 load cart test weight was 269,560 lb, and individual wheel loads were approximately 44,930 lb across two triple wheels in tandem gear (6 tires total). The gear used 50-in.-diam; 21-in.-wide; 20-ply tires maintained at a normal operating pressure of between 138 and 144 psi (Figure 20). The C-17 trafficking followed an approximated normal distribution centered on the crater repair as displayed in Figure 21.

Figure 18. F-15E load cart.

Figure 19. F-15E trafficking distribution.

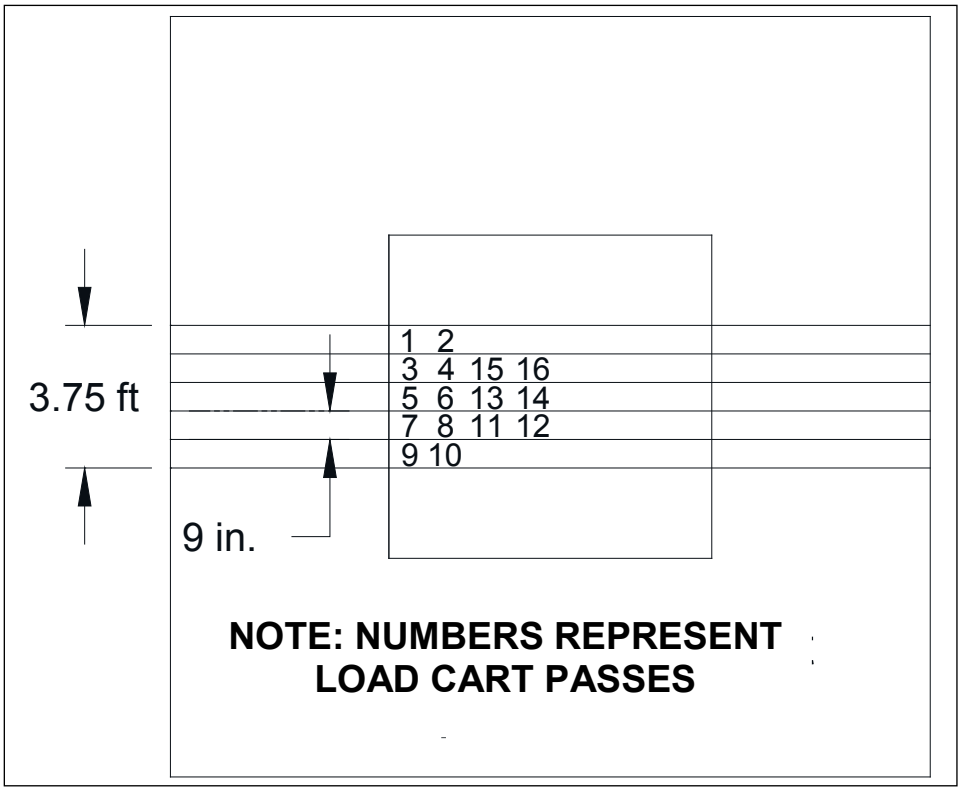

Figure 20 . C-17 load cart.

Figure 21. C-17 trafficking layout.

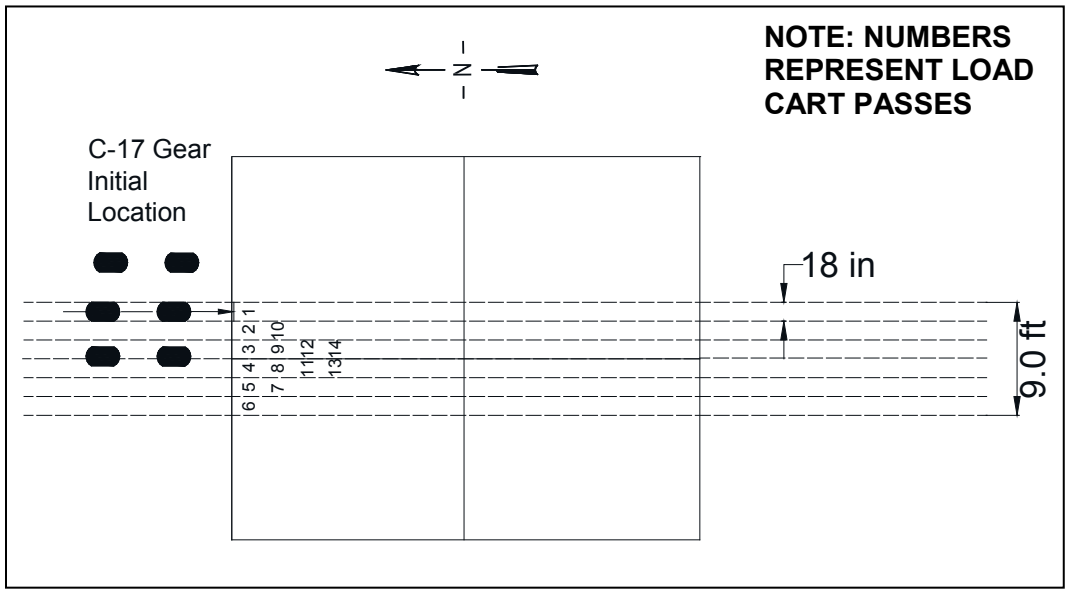

Traffic was applied approximately 2 hr after the last crater in each sequence was completed. Craters 1, 2, and 3 were trafficked simultaneously before these repairs were removed and the remaining excavations reused to create Craters 4, 5, and 6, which were also trafficked simultaneously. The initial 112 passes were applied to Crater 7 approximately 2 hr after the repair was completed. The next day, after Crater 8 was placed and allowed to cure for 2 hr, 112 passes were immediately applied only to Crater 8. Afterwards, trafficking commenced on Craters 7 and 8 simultaneously.

4.4.2 Visual observations before traffic

Before trafficking commenced, each crater was inspected to document any existing distresses. Figure 22 shows Crater 1 before traffic was applied. As

shown, some small deficiencies and a small hole where a DCP test was attempted are visible on the surface. In Figure 23, the surface of Crater 2 shows fewer surface deficiencies but also shows some darker areas around the edge of the crater where the material has likely not reached the same curing level as the center of the crater. These darker areas were no longer visible when trafficking began. Crater 3 exhibited similar characteristics to that of Crater 2, with a much larger area of dark-colored material as shown in Figure 24. However, this dark area was also no longer visible when trafficking began.

Figure 22. Crater 1 before trafficking.

Figure 23. Crater 2 before trafficking.

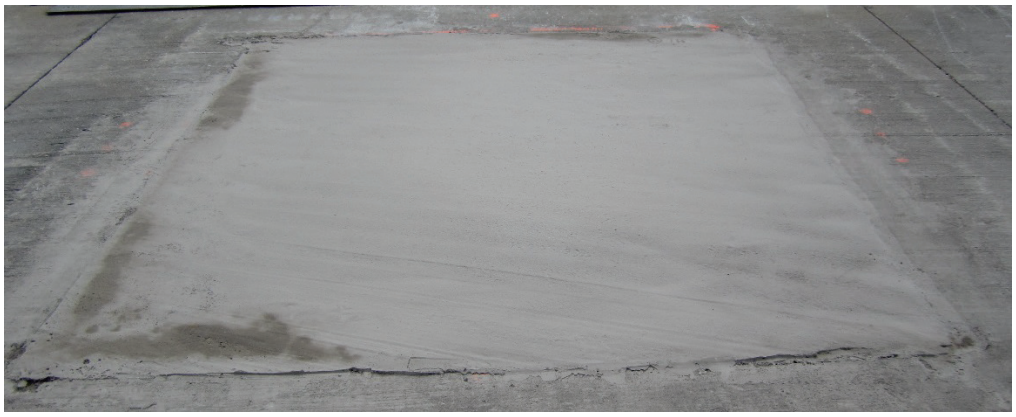

Figure 24. Crater 3 before trafficking.

Figure 25 shows Crater 4 just after screeding and before trafficking. Craters 5 and 6 had a similar appearance. Craters 4, 5, and 6 in general exhibited fewer distresses than Craters 1, 2, and 3. The w/c ratio was decreased by increasing the gate setting on the mixer, resulting in a more viscous and higher strength mix. The w/c ratio changes are discussed further in upcoming paragraphs.

Figure 25. Crater 4 before trafficking.

Figure 26 shows Crater 7 before trafficking. Some minor surface deficiencies were visible near the edge of the crater, but no cracking was observed. A photo of Crater 8 before trafficking is shown in Figure 27. An inset in Figure 27 shows a 0.5-in. deep depression that was created during heavy-weight deflectometer (HWD) testing. Upon further investigation, it was concluded that this test location was a very isolated area of weaker material, since the other two HWD tests on the repair did not result in any depressions. This conclusion was confirmed during trafficking.

Figure 26. Crater 7 before trafficking.

Figure 27. Crater 8 before trafficking.

4.4.3 Visual observations under traffic

After the initial 112 passes (7 complete patterns) were applied to Craters 1, 2, and 3, the craters were again visually examined for damage. Figure 28 shows Crater 1 after 112 passes. The only visible distress was a considerable amount of very small debris (Figure 29). The small debris is discussed further in the next section.

Figure 30 shows a small depression on Crater 2 after 112 passes, along with the small debris mentioned previously. Figure 31 shows an overall photograph and Figure 32 shows a depression on Crater 3 after 112 passes. Two of these depressions were observed on Crater 3, one on the north edge of the crater and one on the south edge (traffic direction was north to south). As with Crater 1 and 2, the depression and accompanying debris were believed to be caused by the abrasive action of the high pressure F-15E load cart tire. Depressions observed on Craters 1 to 3 were approximately 0.25 in. in depth.

Figure 28. Crater 1, 112 passes, overall.

Figure 29. Closeup of small debris on Crater 1 after 112 passes.

Figure 30. Crater 2, 112 passes, depression

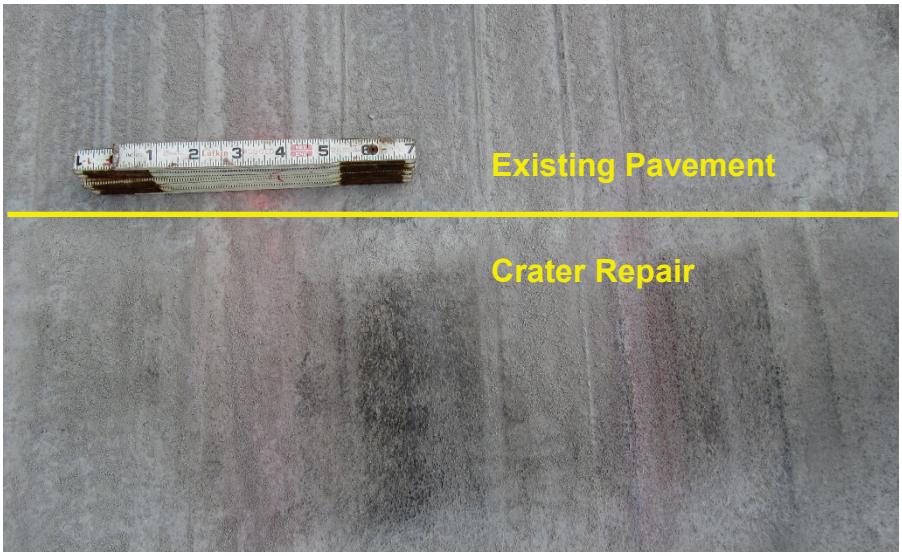

Figure 31. Crater 3, 112 passes, overall.

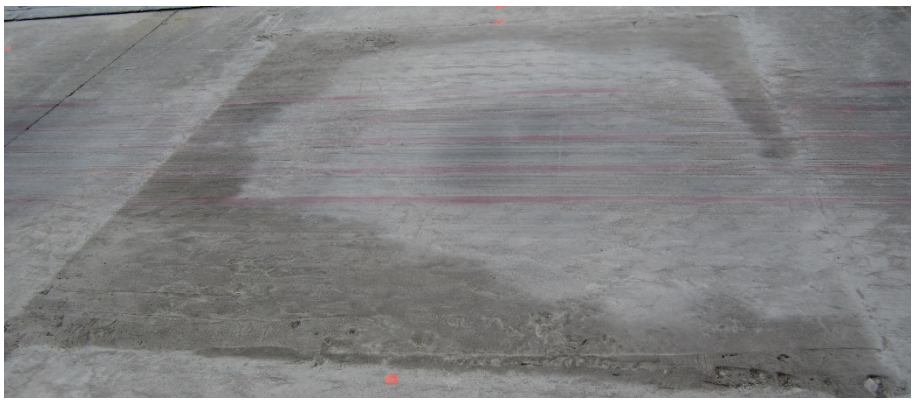

Figure 32. Crater 3, 112 passes, depression.

Each crater was visually inspected every 112 passes going forward. For each visual inspection, the debris was removed with a gas-powered blower after overall photographs were taken so that cracking, spalling, and other similar distresses could be more easily identified. The only significant change in distress between pass 112 and 512 for Craters 1, 2, and 3 was low-severity transverse cracking that began to develop on the south edge of Crater 3 (Figure 33). Also, a considerable amount of the small debris previously discussed continued to be apparent on all repairs during visual observations after every 112 passes.

Figure 33. Crater 3, 224 passes, low-severity transverse crack.

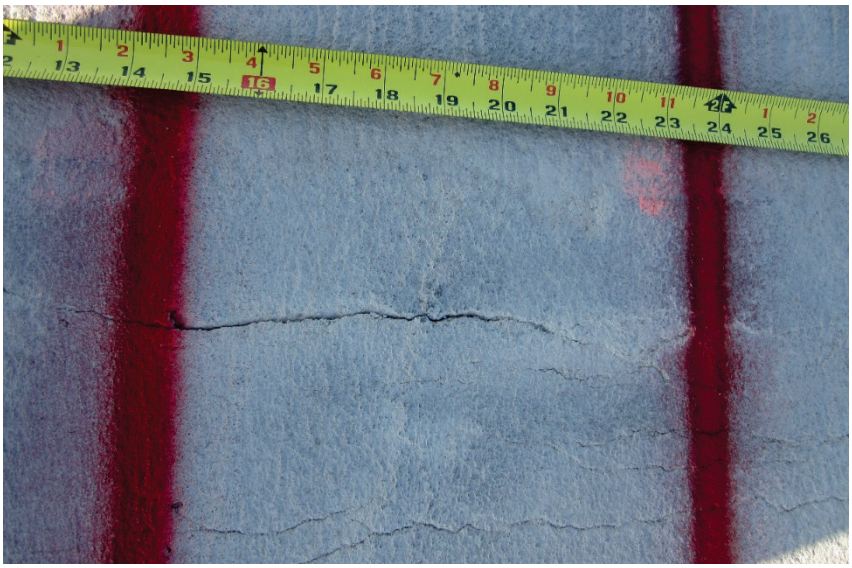

After 512 passes, several notable distresses became apparent. As shown in Figure 34, Crater 1 exhibited medium-severity joint spalling with a high foreign object debris (FOD) potential on the south edge of the repair. Figure 35 shows high-severity joint spalling on the south edge of Crater 2. Some FOD was observed outside the crater and the depth of the spall measured approximately 1 in. The distresses for Crater 3 were less severe; only a depression and medium-severity spalling were observed (Figure 36). Due to the tire hazard created by the high-severity joint spalling, Crater 2 was considered failed. Since Craters 1, 2, and 3 were to be excavated so that Crater repairs 4, 5, and 6 could be constructed, trafficking of Craters 1 and 3 was also ceased.

Figure 34. Crater 1, 512 passes, medium-severity joint spalling.

Figure 35. Crater 2, 512 passes, high-severity joint spalling.

Figure 36. Crater 3, 512 passes, medium joint spalling and depression.

Severe edge spalling is the typical mode of failure exhibited by craters repaired with conventional USAF ADR capping materials (rapid-setting concrete). Since there is no load transfer mechanism (i.e., dowels, rebar), the bond strength between the repair material and the parent slab is the limiting factor when it comes to the failure of the crater repair. Since no distresses that are typically associated with structural failure (faulting, shattered slabs) were observed, it can be reasonably assumed that the thickness of rapid-setting flowable fill was sufficient.

After Craters 1, 2, and 3 were excavated and Crater repairs 4, 5, and 6 were constructed, trafficking commenced. Each repair was inspected every 112 passes; however, no distresses were noted, and much less small debris was observed compared to Craters 1, 2, and 3. Figure 37 shows debris accumulating on Crater 4 after 112 passes. Craters 5 and 6 showed a smaller amount of debris compared to Crater 4. Trafficking was ceased at 512 passes due to limited time on the test site, but no notable distresses were observed. Figure 38 shows an overall photograph of Craters 4, 5, and 6 after 512 passes. The reduction in distresses could be due to a slight decrease in the w/c ratio that was implemented for Craters 4, 5, and 6 and discussed previously in Section 3.3.

For Craters 7 and 8, visual inspections were conducted every 28 passes and any noteworthy distresses were recorded. As shown in Figure 39, a network of low-severity cracking began to develop on Crater 7 after 84 passes (shown in yellow). After 112 passes, low-severity joint spalling was observed near this network of cracking, and more cracks were developed as shown in Figure 40.

Figure 37. Crater 4, 512 passes, small debris.

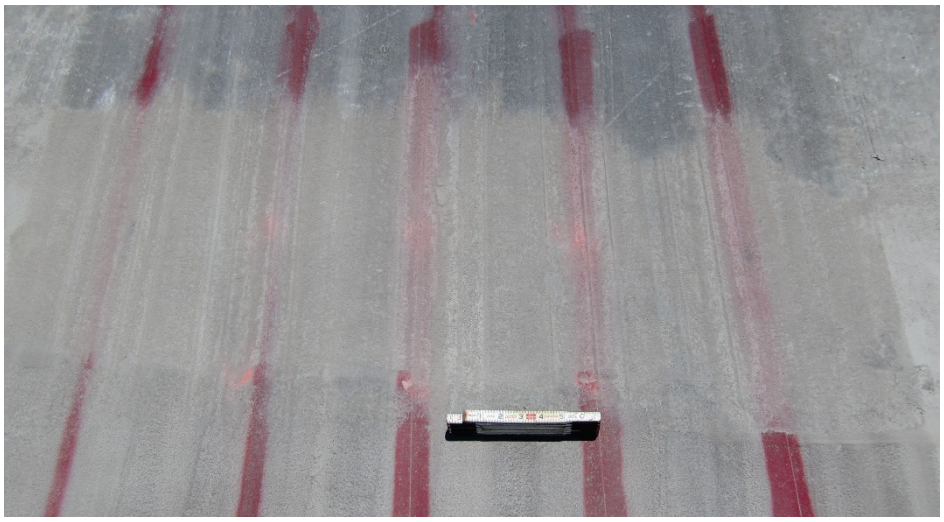

Figure 38. Craters 4, 5, and 6, 512 passes, overall.

Figure 39. Crater 7, 84 passes, low-severity cracking.

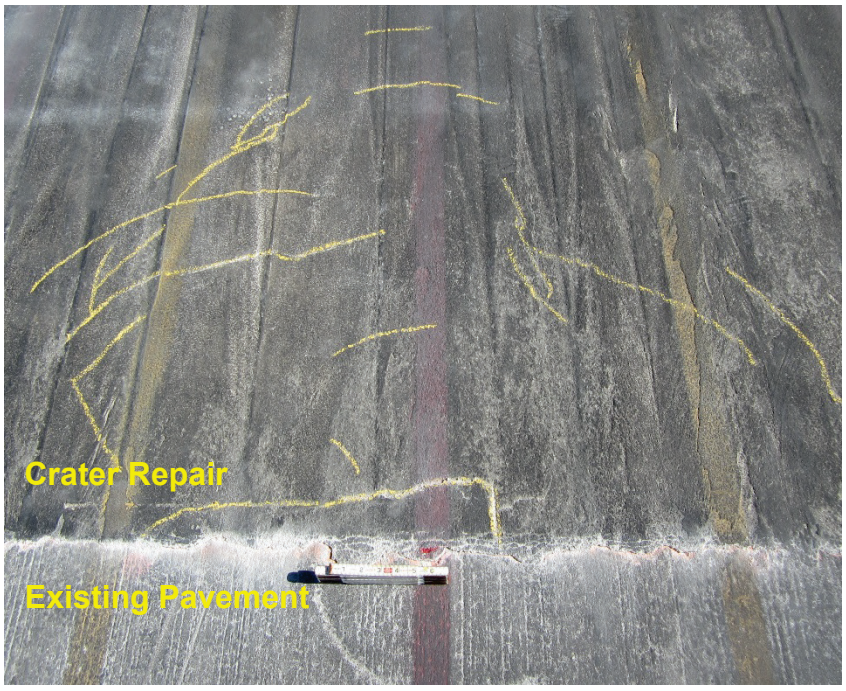

Figure 40. Crater 7, 112 passes, low-severity joint spalling and cracking.

Figure 41 shows the north edge of Crater 7 after 224 passes. The low-severity joint spalling had progressed into high-severity joint spalling, and the network of smaller cracks continued to develop. Figure 42 shows Crater 7 at failure, after 504 passes. On the north edge, the area of low-severity cracking continued to expand, and the spalling along the edge extended to span the entire width of the traffic lanes. The south edge exhibited only a few low-severity transverse cracks as shown in Figure 43, a sharp contrast to the distress observed on the north edge of Crater 7. Trafficking ceased after 504 passes.

Figure 44 shows the south edge of Crater 8 after 112 passes. Some low-severity transverse cracking and joint spalling was observed. After 224 passes, a low-severity depression with low-severity cracking surrounding the depression was observed (Figure 45). After 224 passes, a larger network of cracks was apparent, and the spall width had increased, as shown in Figure 46. After 504 passes, high-severity joint spalling was observed on both the south edge (Figure 47) and the north edge (Figure 48). On the south edge, some delamination of the surface was observed as shown on the inset of Figure 48. Possible causes of the delamination are discussed in the next section. Trafficking was ceased after 504 passes.

Figure 41. Crater 7, 224 passes, high-severity joint spalling on north edge.

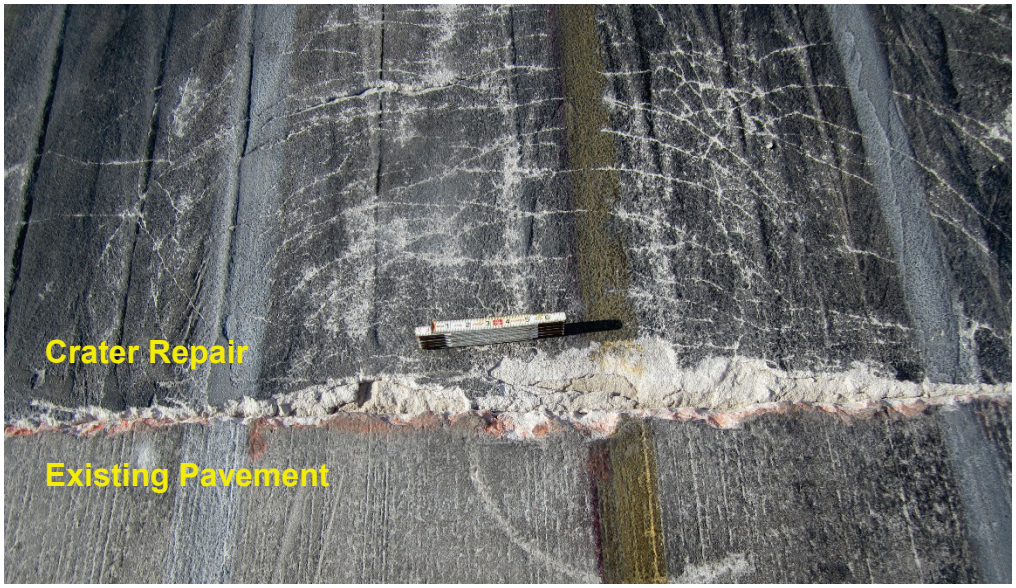

Figure 42. Crater 7, 504 passes, high-severity joint spalling on north edge.

Figure 43. Crater 7, 504 passes, south edge.

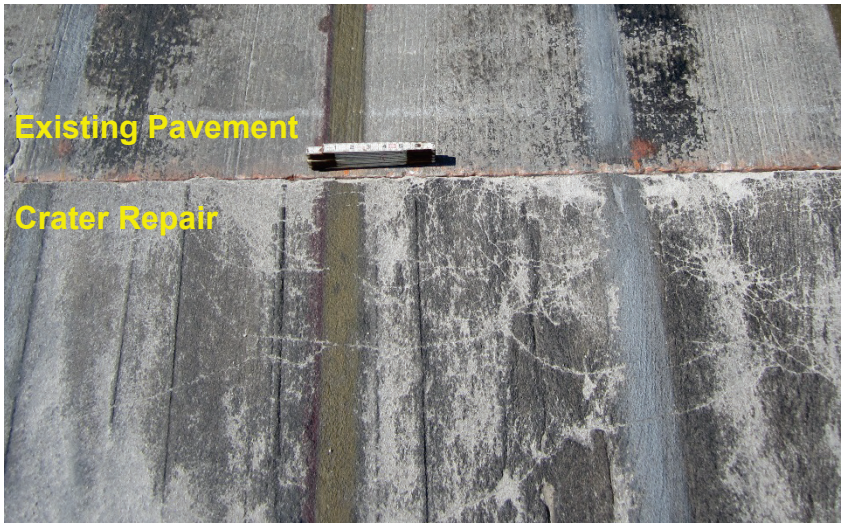

Figure 44. Crater 8, 112 passes, distresses on south edge.

Figure 45. Crater 8, 224 passes, low-severity cracking and depression.

Figure 46. Crater 8, 224 passes, distresses on south edge.

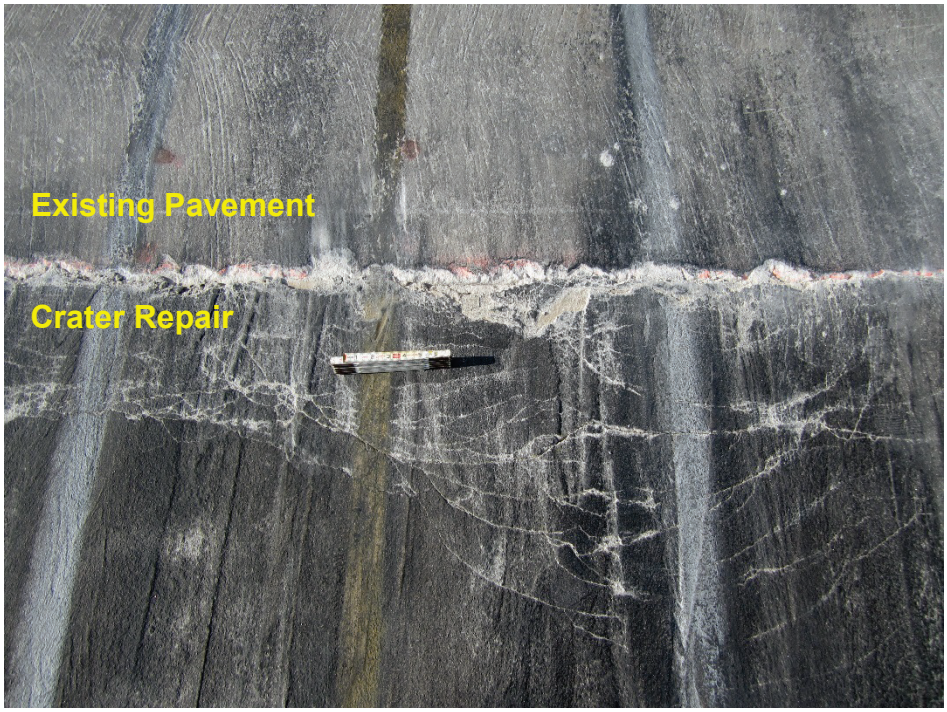

Figure 47. Crater 8, 504 passes, high-severity spalling on south edge.

Figure 48. Crater 8, 504 passes, high-severity spalling on north edge.

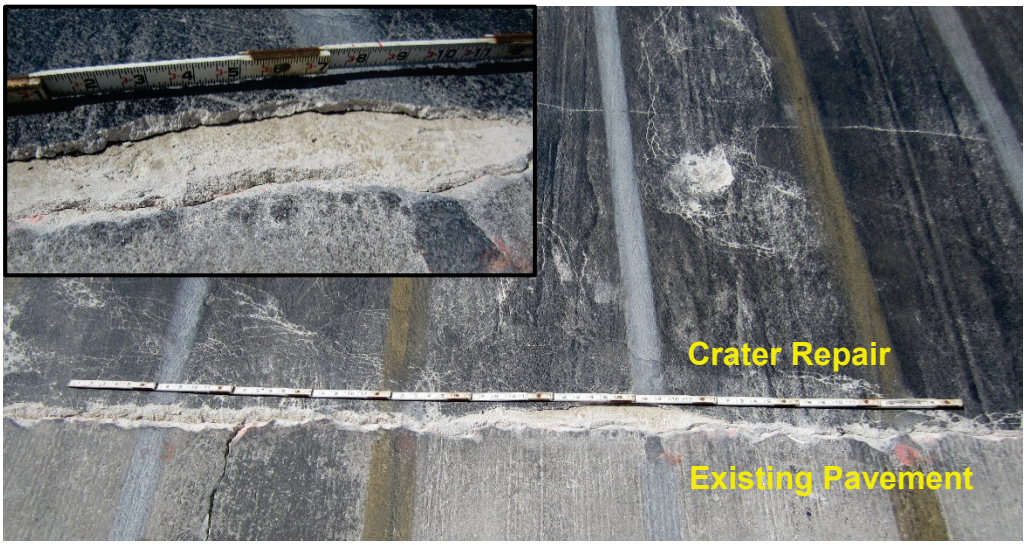

4.4.4 Discussion of distresses observed under traffic

Under traffic, rapid-setting flowable fill exhibited many of the same characteristics as other stabilized materials such as cement-stabilized soil. A considerable amount of small dust-like debris was noted during trafficking, and some depressions were observed due to the abrasive action of aircraft loads with high tire pressures. Moreover, small depressions were occasionally observed. A sample of the small debris was collected and subjected to a sieve analysis to determine the size of the debris. The results of the sieve analysis are shown in Table 12. Nearly all the debris was 0.04 in. (1 mm) in diameter or smaller in size. The small debris would likely not be a FOD concern for large cargo aircraft, but if fighter aircraft are operating on the airfield surface, the amount of debris should be monitored. Periodic sweeping should be used to remove any debris during aircraft operations. Also, the jet blast from normal aircraft operations could prevent the debris from collecting at all, in which case the amount of sweeping required would likely be reduced.

In addition to the smaller depressions previously described that were created by the abrasive action of the load cart wheel, some isolated areas of weaker material were noted on Craters 7 and 8. Some weaker areas were recorded as depressions near the center of the crater, while some were observed near the crater edges (delamination shown in Figure 48). These areas of weaker material were likely caused by placing a more fluid material (higher w/c ratio) for the large craters as discussed previously in Section 3.3.

Table 12. Grain size distribution of flowable fill trafficking debris.

Sieve #	Opening (in.)	Opening (mm)	Percent Finer (%)
10	0.187	4.75	100
16	0.046	1.18	98.1
20	0.034	0.850	80.3
30	0.023	0.595	51.7
40	0.016	0.425	30.8
50	0.012	0.297	21.4
70	0.008	0.212	17.5
100	0.006	0.149	15.7
140	0.004	0.105	14.8
200	0.003	0.074	14.2

None of the crater repairs described in this report showed evidence of structural failure (i.e., shattered slab) at the conclusion of trafficking. The mode of failure was typically high-severity spalling at joints perpendicular to the direction of traffic. This mode of failure is typical for these types of crater repairs as discussed in Priddy et al. (2016). The reason for this failure mode is the lack of load transfer between the crater repair and the parent slab. The bond strength between the repair material and the parent slab is the limiting factor in determining the durability of the crater repair. Although no specific failure criteria were used in this report, it is recommended that further investigations into using rapid-setting flowable fill use the same failure criteria utilized by Priddy et al. (2016), since that failure criteria was used to develop performance curves for conventional USAF cementitious capping materials (rapid-setting concrete). The failure criteria used by Priddy et al. (2016) defined failure as a high-severity shattered slab or spalling greater than 2 ft long, greater than 6 in. wide, and greater than 2 in. deep across 50 percent of the spall length. Similar performance curves could be developed for rapid-setting flowable fill as a capping material, and using the same failure criteria would be beneficial in order to maintain consistency.

4.4.5 Surveying layout and test results

Elevation surveys were performed to: 1) measure repair layer thicknesses; and 2) assess damage over time from aircraft trafficking. Particular attention was paid to the edges of a crater as failures are prone to occur at the edges due to a lack of load transfer. With regard to trafficking damage, an elevation difference of 0.75 in. or greater between the crater and

surrounding pavement was set as a failure criteria, since this elevation difference is a roughness requirement for fighter aircraft such as the F-15. The elevation difference was primarily measured to assess faulting and/or settlement of the entire crater repair, not to measure voids created due to spalling. Also, the rod used for survey measurements was square-shaped with a flat bottom -- not a point on the bottom. Accordingly, the survey results obtained inside the crater repair near the edges where traffic was applied may contradict the visual observations under traffic discussed in Section 4.4.3, since the deep spalls were likely bridged by the bottom of the rod during survey measurements, and the goal of the surveying measurements was to detect area movement instead of discrete distress characteristics.

Figure 49 shows an 8.5-ft by 8.5-ft crater and depicts the manner in which survey measurements were taken. Recall that Craters 1 to 6 were 8.5 ft by 8.5 ft, and that Craters 7 and 8 were 15 ft by 15 ft. For the 8.5-ft by 8.5-ft craters, four lines were surveyed; three were parallel to the traffic direction, and the fourth (cross section) was perpendicular to traffic. The three lines parallel to traffic were spaced 9 in. apart with the middle line aligning with the center of the crater (i.e., 51 in. from either edge). Each of these three lines align with the aircraft trafficking pattern and are referred to as east, center, and west lines based on their orientation to north.

Figure 49. Example survey schematic for 8.5-ft by 8.5-ft crater (Craters 1 to 6).

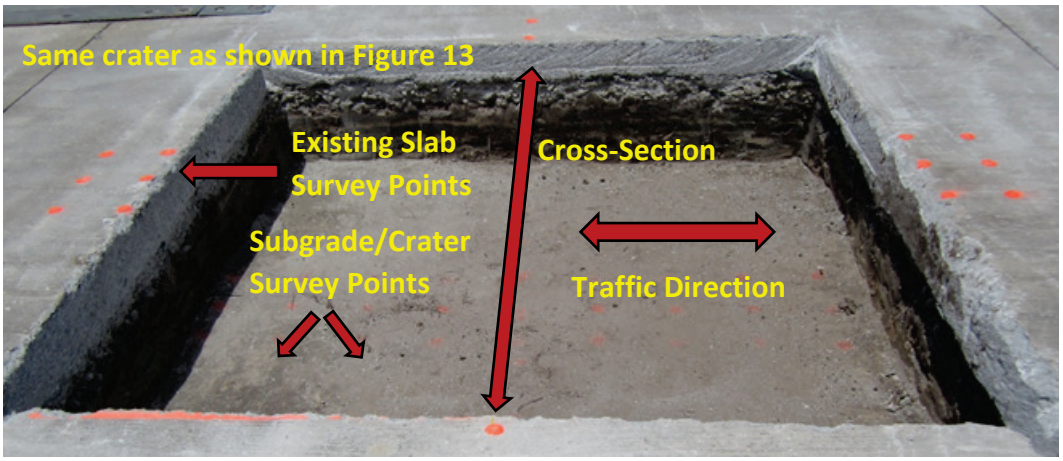

For each line, there were 13 survey coordinates. Four of these 13 coordinates were outside the crater on the existing pavement, as shown in Figure 49 with orange paint dots. On each side of the crater, one coordinate was 12 in. from the edge of the crater, while the other was 2 in. from the edge of the crater. The elevations of these two coordinates were

averaged to establish the elevation on one side of the crater. Inside the crater there were 9 coordinates (also shown in Figure 49 but with less visible paint dots). Two of these 9 coordinates were 2 in. from the crater's edge, with the remaining seven coordinates spaced around 12 in. apart.

For the 8.5-ft by 8.5-ft craters, data collected from each of the 13 coordinate lines surveyed were interpreted as follows. The side of the crater with the highest average elevation was used as a reference zero elevation, and all other data were compared to this elevation (positive values being higher than this location and negative values being lower than this location). Reducing survey data in this manner introduces a slightly overstated crater layer thickness, which can be interpreted in the context of the elevation difference between one side of the crater to the other, which is referred to hereafter as outer elevation difference (OED). Generally speaking, half of the OED is a reasonable estimate for the thickness overestimation occurring from this approach. For surveys where crater layer thicknesses were determined, all 36 data points were evaluated as a single data set and the average (Avg), minimum (Min), maximum (Max), and standard deviation (St.Dev.) of thicknesses were reported along with the OED. For surveys where the crater surface was surveyed after different pass levels, the same terms were reported, except each line's data was kept separate. Layer thicknesses for all eight craters are provided in Table 13 (note that descriptions of Craters 7 and 8 are described later in this section), and Craters 1 to 6 surface profile results are provided in Table 14, Table 15, and Table 16.

Craters 1 to 3 are described together in Table 14 as they are the three 8.5-ft by 8.5-ft craters evaluated without any base material. With regard to data evaluation, the East, Center, and West lines are, generally speaking, more indicative of traffic damage at the edges since they are parallel to traffic. Also, relative differences from 0 to 112 passes and then from 112 to 512 passes was deemed the best indicator of traffic damage, since construction quality is largely independent of traffic damage. The "overall" row lists the greatest change in elevation between any two pass levels (positive for an increase in elevation for a decrease in elevation level). Crater 1 did not experience changes nearing 0.75 in. due to traffic when considering the overall row. For example, the East line had average values within 0.04 in. of each other, and the Min and Max readings between pass levels never differed by more than 0.06 in. Crater 2 results were similar to Crater 1 in that no overall row readings exceeded the 0.75-in. threshold. Crater 2's

cross-section profile at 112 passes did not align well with values at 0 and 512 passes but, even so, the overall readings were all less than 0.75 in. Crater 3's overall readings align with Crater 1 in that all readings were well below the 0.75-in. threshold.

Table 13. Layer thicknesses measured via elevation surveys.

Crater	Avg (in.)	Min (in.)	Max (in)	St.Dev. (in.)	OED (in.)
1-FF Cap	19.9	19.0	20.8	0.39	0.30
2- FF Cap	22.1	21.5	22.6	0.24	0.31
3- FF Cap	24.2	23.4	25.0	0.33	0.41
4-Total Crater Depth	23.7	22.1	24.7	0.55	0.35
4-Backfill	11.8	10.8	12.5	0.38	0.33
4-FF Cap	11.9	---	---	---	---
5-Total Crater Depth	22.1	20.8	23.2	0.54	0.41
5-Backfill	11.4	10.8	11.9	0.25	0.38
5-FF Cap	10.7	---	---	---	---
6- Total Crater Depth	24.0	23.2	24.8	0.39	0.33
6-Backfill	11.9	11.3	12.9	0.34	0.33
6-FF Cap	12.1	---	---	---	---
7-FF Cap	24.3	23.0	25.5	0.46	0.50
8-Total Crater Depth	23.5	22.7	23.9	0.25	0.48
8-Backfill	12.6	11.6	13.3	0.42	0.50
8-FF Cap	10.9	---	---	---	---

Table 14. Craters 1, 2, and 3 surface profiles measured via elevation surveys.

Crater	Line	Passes	[a]Avg (in.)	[a]Min (in.)	[a]Max (in.)	[a]St.Dev. (in.)	OED (in.)
1	East	0	0.01	-0.06	0.06	0.06	0.18
1	East	112	0.05	-0.12	0.12	0.09	0.06
1	East	512	0.01	-0.06	0.06	0.06	0.12
1	Center	0	0.03	0.00	0.12	0.05	0.12
1	Center	112	0.11	0.00	0.12	0.04	0.00
1	Center	512	-0.01	-0.12	0.00	0.04	0.12
1	West	0	-0.04	-0.12	0.00	0.06	0.18
1	West	112	0.00	-0.12	0.12	0.08	0.12
1	West	512	0.03	-0.12	0.12	0.08	0.12
1	Cross-Section	0	-0.21	-0.66	0.18	0.34	0.72
1	Cross-Section	112	-0.18	-0.66	0.06	0.27	0.78

Crater	Line	Passes	[a]Avg (in.)	[a]Min (in.)	[a]Max (in.)	[a]St.Dev. (in.)	OED (in.)
1	Cross-Section	512	-0.15	-0.66	0.18	0.29	0.72
1[b]	**Overall**	**—**	**0.12**	**-0.12**	**0.12**	**—**	**—**
2	East	0	0.14	0.06	0.18	0.06	0.12
2	East	112	0.17	0.00	0.24	0.09	0.12
2	East	512	0.19	0.00	0.24	0.09	0.12
2	Center	0	0.17	0.12	0.24	0.06	0.12
2	Center	112	0.07	-0.24	0.12	0.12	0.18
2	Center	512	0.14	-0.06	0.18	0.08	0.12
2	West	0	0.14	0.06	0.18	0.06	0.12
2	West	112	0.09	-0.12	0.12	0.08	0.18
2	West	512	0.09	0.00	0.12	0.05	0.12
2	Cross-Section	0	-0.17	-0.54	0.06	0.18	1.02
2	Cross-Section	112	-0.61	-0.90	-0.42	0.16	1.44
2	Cross-Section	512	-0.21	-0.48	0.00	0.17	0.96
2[b]	**Overall**	**—**	**-0.44**	**-0.42**	**-0.48**	**—**	**—**
3	East	0	0.04	-0.12	0.12	0.10	0.12
3	East	112	-0.07	-0.48	0.12	0.19	0.24
3	East	512	-0.05	-0.36	0.12	0.15	0.24
3	Center	0	-0.04	-0.24	0.12	0.16	0.24
3	Center	112	-0.07	-0.48	0.12	0.22	0.24
3	Center	512	-0.01	-0.42	0.18	0.22	0.30
3	West	0	-0.05	-0.42	0.06	0.16	0.24
3	West	112	-0.13	-0.66	0.06	0.26	0.36
3	West	512	-0.07	-0.60	0.12	0.25	0.24
3	Cross-Section	0	-0.22	-0.78	0.06	0.31	0.84
3	Cross-Section	112	-0.40	-0.84	-0.12	0.23	0.96
3	Cross-Section	512	-0.29	-0.78	-0.06	0.27	0.84
3[b]	**Overall**	**—**	**-0.18**	**-0.36**	**-0.18**	**—**	**—**

[a] Negative values are below the datum point, positive values are above the datum point.

[b] Overall refers to the maximum change (positive or negative) between any two pass levels for the referenced line.

Table 15 provides surface profile results for Crater 4, which is the only crater that was 8.5 ft by 8.5 ft and had masonry sand backfill. Only two survey readings were taken (0 and 512 passes). None of the overall row readings had changes of 0.75 in., which agrees with Craters 1, 2, and 3 in an overall sense.

Table 15. Crater 4 surface profile measured via elevation surveys.

Crater	Line	Passes	[a]Avg (in.)	[a]Min (in.)	[a]Max (in.)	[a]St.Dev. (in.)	OED (in.)
4	East	0	0.11	-0.12	0.36	0.16	0.24
4	East	512	0.20	0.00	0.48	0.17	0.06
4	Center	0	0.25	0.00	0.48	0.20	0.18
4	Center	512	0.20	-0.12	0.48	0.20	0.18
4	West	0	0.19	-0.12	0.48	0.23	0.24
4	West	512	0.24	-0.12	0.48	0.22	0.18
4	Cross-Section	0	0.03	-0.54	0.42	0.34	0.78
4	Cross-Section	512	-0.10	-0.78	0.30	0.38	0.96
4[b]	Overall	---	-0.13	-0.24	-0.12	---	---

[a]Negative values are below the datum point, positive values are above the datum point.

[b]Overall refers to the maximum change (positive or negative) between any two pass levels for the referenced line.

Table 16 provides Crater 5 and 6 surface profile results, which are the two craters that are 8.5 ft by 8.5 ft and have crushed stone backfill. No Crater 5 overall row readings were close to exceeding the 0.75-in. threshold when comparing 0 passes to 512 passes. Crater 6 behaved similarly to Crater 5, and there were no overall readings that approached the 0.75-in. threshold.

Craters 7 and 8 were the only craters that were 15 ft by 15 ft. Crater 7 had full depth flowable fill, while Crater 8 had 12 in. of crushed stone backfill and 12 in. of rapid-setting flowable fill. The same concept was used to collect elevation measurements for 15-ft craters as for 8.5-ft craters. Procedurally, though, there were some differences for the 15-ft craters: 1) 19 measurements were taken per line instead of 13, with 6 more interior measurements but the same pattern outside the crater and near the edges; 2) five lines were surveyed instead of four (cross section, East, Center 1, Center 2, and West), and 3) the five lines were spaced 18 in. apart. The lines were spaced 18 in. apart to match the width of the C-17 load cart tire, and the four lines were centered in the four middle traffic lanes. Data reduction was conducted in the same manner as with the 8.5-ft by 8.5-ft craters.

Table 16. Craters 5 and 6 surface profiles measured via elevation surveys.

Crater	Line	Passes	[a]Avg (in.)	[a]Min (in.)	[a]Max (in.)	[a]St.Dev. (in.)	OED (in.)
5	East	0	0.08	-0.12	0.24	0.10	0.18
5	East	512	0.10	-0.06	0.18	0.08	0.12
5	Center	0	0.03	-0.24	0.24	0.13	0.24
5	Center	512	0.05	-0.12	0.24	0.11	0.18
5	West	0	0.04	-0.12	0.24	0.10	0.18
5	West	512	0.13	0.00	0.24	0.09	0.12
5	Cross-Section	0	-0.30	-0.78	-0.06	0.26	1.02
5	Cross-Section	512	-0.34	-0.90	-0.06	0.28	1.08
5[b]	**Overall**	**—**	**0.09**	**-0.12**	**-0.06**	**—**	**—**
6	East	0	0.28	0.12	0.48	0.13	0.06
6	East	512	0.23	0.00	0.36	0.13	0.12
6	Center	0	0.21	0.00	0.36	0.16	0.06
6	Center	512	0.23	0.00	0.36	---	---
6	West	0	0.21	-0.06	0.42	0.16	0.06
6	West	512	0.21	-0.06	0.42	0.14	0.18
6	Cross-Section	0	-0.15	-0.78	0.18	0.33	0.96
6	Cross-Section	512	-0.19	-0.78	0.18	0.35	0.96
6[b]	**Overall**	**—**	**-0.05**	**-0.12**	**-0.12**	**—**	**—**

[a]Negative values are below the datum point, positive values are above the datum point.

[b]Overall refers to the maximum change (positive or negative) between any two pass levels for the referenced line.

Table 17 provides survey results for Craters 7 and 8. Crater 7 does not have any row readings outside the 0.75-in. threshold when viewed as a function of passes, but the cross section has a noticeable slope (i.e., high OED). Crater 8 agrees with Crater 7, but there is a large discrepancy in Min values (0.72-in.) between 0 and 504 passes. To investigate this further, Figure 50 plots normalized survey coordinates versus distance along the cross section (one side of the cross section being arbitrarily labeled 0 in.) for Crater 7, and Figure 51 plots the same data for Crater 8. When the profiles are plotted, it becomes clear that there is a fairly continuous cross-section profile and that there is only one instance where the 0.75-in. threshold is approached. This instance was observed at 0 passes in Crater 8 between 0 and around 18 in. from the edge of the crater arbitrarily labeled 0. This measurement was not repeated at later passes, likely meaning this difference was measurement error and not an issue with the crater edge violating the 0.75-in. threshold.

Table 17. Craters 7 and 8 surface profiles measured via elevation surveys.

Crater	Line	Passes	[a]Avg (in.)	[a]Min (in.)	[a]Max (in.)	[a]St.Dev. (in.)	OED (in.)
7	East	0	0.07	0.00	0.12	0.06	0.12
7	East	112	0.12	0.00	0.24	0.06	0.06
7	East	504	0.12	-0.12	0.24	0.09	0.12
7	Center 1	0	-0.02	-0.12	0.00	0.05	-0.06
7	Center 1	112	0.04	0.00	0.12	0.06	0.00
7	Center 1	504	0.02	0.00	0.12	0.04	0.00
7	Center 2	0	0.02	0.00	0.12	0.04	0.06
7	Center 2	112	0.11	0.00	0.24	0.05	0.00
7	Center 2	504	0.09	-0.12	0.12	0.07	0.00
7	West	0	-0.05	-0.12	0.00	0.06	0.48
7	West	112	-0.06	-0.12	0.00	0.06	0.06
7	West	504	0.07	0.00	0.12	0.06	0.00
7	Cross-Section	0	-0.54	-1.32	0.00	0.44	-1.56
7	Cross-Section	112	-0.55	-1.44	0.00	0.46	-1.62
7	Cross-Section	504	-0.61	-1.38	-0.06	0.45	-1.62
7[b]	Overall	---	-0.06	-0.12	0.12	---	---
8	East	0	-0.07	-0.12	0.00	0.06	-0.18
8	East	112	-0.06	-0.12	0.00	0.06	-0.18
8	East	504	-0.02	-0.12	0.00	0.05	-0.12
8	Center 1	0	-0.13	-0.30	-0.06	0.09	-0.30
8	Center 1	112	-0.17	-0.24	0.00	0.08	-0.36
8	Center 1	504	-0.10	-0.36	0.00	0.11	-0.24
8	Center 2	0	-0.14	-0.24	0.00	0.09	-0.24
8	Center 2	112	-0.14	-0.36	0.00	0.11	-0.24
8	Center 2	504	-0.08	-0.24	0.00	0.07	-0.24
8	West	0	-0.02	-0.12	0.12	0.08	-0.24
8	West	112	-0.05	-0.18	0.06	0.10	-0.30
8	West	504	-0.06	-0.36	0.00	0.10	-0.24
8	Cross-Section	0	-0.50	-1.92	-0.12	0.46	-1.74
8	Cross-Section	112	-0.49	-1.20	0.00	0.36	-1.44
8	Cross-Section	504	-0.38	-1.20	0.12	0.38	-1.32
8[b]	Overall	---	-0.12	-0.72	0.24	---	---

[a]Negative values are below the datum point, positive values are above the datum point.

[b]Overall refers to the maximum change (positive or negative) between any two pass levels for the referenced line.

Figure 50. Crater 7 cross-section normalized profiles.

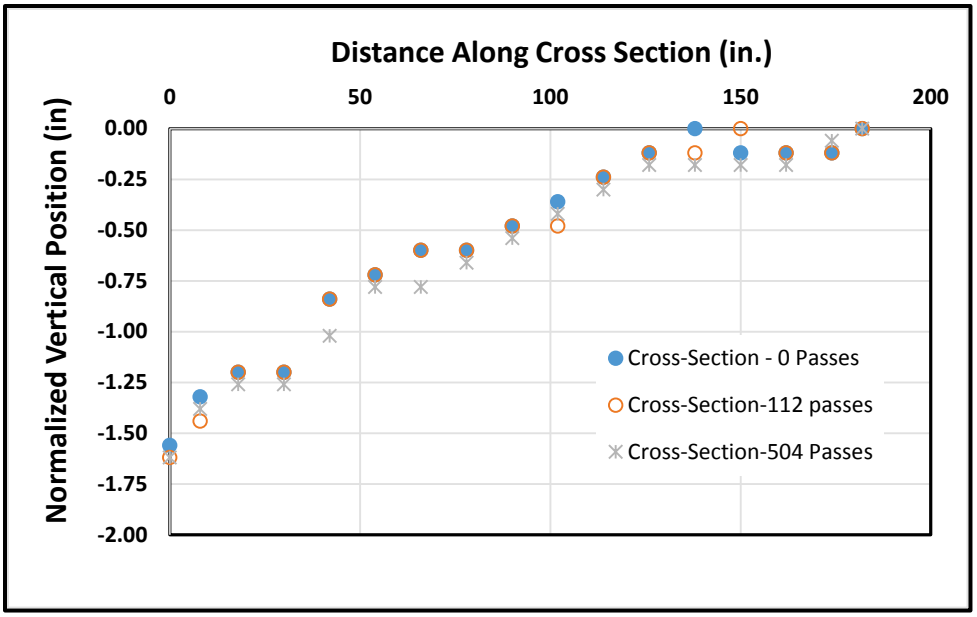

Figure 51. Crater 8 cross-section normalized profiles.

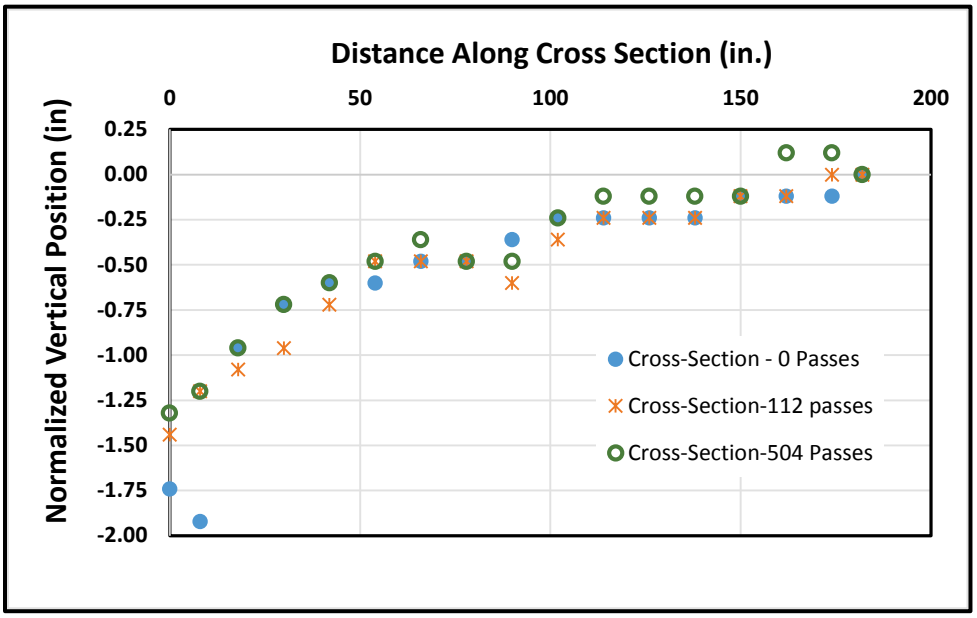

Overall, the survey data indicated that all 8 craters performed satisfactorily in terms of their ability to maintain a surface profile while being tracked with fighter or cargo aircraft. In most cases, deviations were much lower than the 0.75-in. threshold. Thus, there was little concern with potential roughness issues for craters repaired with rapid-setting flowable fill.

4.5 Heavy-weight deflectometer test results and analysis

4.5.1 Testing and analysis technologies

Heavy-weight deflectometer (HWD) testing occurred on each crater prior to trafficking (0 passes) and after 504 (C-17) or 512 (F-15) passes. Time between 0-pass HWD testing and the completion of rapid-setting flowable fill placement was approximately 2 hr. The time between 0 to 512 pass (or 504 pass) intervals was less than 48 hr, but was during the early-age period for the cementitious materials.

HWD testing was performed primarily to characterize the stiffness of rapid-setting flowable fill, to investigate trends, and to provide an independent behavioral assessment. On site there was no monitoring of hydration progression that could be coupled with the FWD measurements. All other factors being equal: 1) deflection would be expected to decrease (or perhaps stay the same) as hydration progressed over time; and 2) deflection would be expected to increase (or perhaps stay the same) as traffic progressed. In that there were no parallel sections built absent traffic and tested with the HWD over time, there was no direct mechanism with which to decouple these behaviors. This does not negate the usefulness of HWD data for trends identification, but should be understood when interpreting findings presented in the remainder of this section.

HWD testing was performed by measuring deflection (D) at seven locations (D_1 to D_7) relative to the center of the load plate. D_i locations were as follows relative to the center of the load plate: D_1 = 0 in., D_2 = 12 in., D_3 = 24 in., D_4 = 36 in., D_5 = 48 in., D_6 = 60 in., D_7 = 72 in. The load plate was 11.8 in. in diameter, and contact pressures were typically between 375 and 525 psi, with most testing being on the order of 500 psi (55 kips). At each location, the HWD was dropped four times without re-location. HWD testing before and after traffic occurred at essentially the same location. For Craters 1 to 6, one location was tested per crater; for Craters 7 and 8 (15-ft by 15-ft craters), three locations were tested.

Upon visual examination of the data collected, tremendous variability was evident in a few cases. Cases where variability was apparent seemed to be associated with one of two situations that are not intuitive: 1) D_1 increases considerably between successive drops without a corresponding increase in applied HWD stress; or 2) there was not a trend of decreasing D_1 with decreasing applied HWD stress. Cases where data were collected that were

not deemed reliable based on judgment and application of the aforementioned situations was marked with an (*) in the tables presented in the remainder of this section and were not used for any type of analysis. Once HWD drops deemed unreliable were excluded, HWD measurements at each deflection measurement location (D_1 to D_7) were linearly adjusted to a 500 psi contact stress for comparative discussion (these deflection basins were referred to as *Adj.*). In a few cases, linear adjustment produced unreasonable values when there were only two of the four HWD drops that were useable and, in these cases, a best estimate of a 500 psi adjusted deflection basing was provided (e.g., Crater 6). If one sensor reading was deemed unreliable, the entire HWD drop was omitted from analysis.

4.5.2 HWD deflection basin analysis

Table 18 provides measured HWD deflection basins for Craters 1 to 3, which are the three 8.5-ft by 8.5-ft craters absent backfill. Recall DCP testing was used to estimate CBR values for underlying layers and that there were little to no meaningful differences between the underlying subgrade for Craters 1, 2, and 3. Craters 1 and 2 have essentially the same 500 psi adjusted deflection basins before and after trafficking. Crater 3's after-trafficking deflection basin is modestly higher (3 to 5 mils) than before traffic. Crater 3 appeared to be damaged by traffic (i.e., increased deflection), while Crater 1 and Crater 2 did not appear to be damaged by traffic (deflections did not increase due to traffic), or at least Crater 1 and 2 appeared to experience less damage due to traffic (note that all factors being equal, deflections should decrease as hydration progresses in early ages) than Crater 3, which is not intuitive.

What is also not intuitive is the inverse relationship of deflection to FF cap thickness over an essentially constant subgrade. Before traffic, D_1 values were 13.8, 16.1, and 16.7 mils for flowable fill cap thicknesses of 20, 22, and 24 in., respectively. After traffic, the same trend was observed with D_1 values being 13.6, 15.5, and 19.5 mils for FF cap thicknesses of 20, 22, and 24 in., respectively. It is possible that material property differences between FF caps possibly due to gate setting differences between craters led to the non-intuitive results when comparing Craters 1, 2, and 3.

Table 18. HWD measurements of Craters 1, 2, and 3.

Crater	Passes	HWD Drop	Contact Stress (psi)	Deflection (mils)						
				D_1	D_2	D_3	D_4	D_5	D_6	D_7
1	0	1	499	14.0	11.9	11.0	10.3	9.6	8.4	7.0
		2	507	12.6	10.5	9.7	9.0	8.3	7.1	6.0
		3*	522	29.0	10.2	9.3	8.4	7.9	6.7	5.5
		4*	403	26.4	7.3	6.8	6.4	5.8	4.6	3.8
		Adj	*500*	*13.8*	*11.7*	*10.8*	*10.1*	*9.4*	*8.2*	*6.9*
1	512	1	518	14.3	12.1	11.2	10.7	10.4	6.0	5.1
		2	517	14.1	11.7	11.0	10.5	10.2	6.0	5.2
		3	518	14.1	11.6	10.9	10.4	10.1	6.1	5.1
		4	423	11.1	9.5	8.5	8.1	7.9	4.8	4.0
		Adj	*500*	*13.6*	*11.4*	*10.6*	*10.1*	*9.8*	*5.6*	*4.9*
2	0	1	478	15.9	13.5	12.1	10.8	9.6	8.2	6.8
		2	484	14.8	12.1	10.9	9.7	8.7	7.5	6.3
		3	487	15.2	11.9	10.6	9.5	8.5	7.3	6.0
		4	402	11.2	9.4	8.4	7.4	6.6	5.5	4.6
		Adj	*500*	*16.1*	*13.1*	*11.7*	*10.5*	*9.4*	*9.1*	*6.7*
2	512	1	522	16.8	14.6	13.7	13.2	13.0	5.1	4.2
		2	522	16.2	14.1	13.1	12.5	12.1	5.2	4.3
		3	526	15.7	14.0	12.9	12.3	11.9	5.1	4.2
		4	422	12.8	11.0	10.4	9.5	9.3	3.9	3.2
		Adj	*500*	*15.5*	*13.5*	*12.6*	*11.9*	*11.6*	*4.9*	*4.0*
3	0	1	502	16.5	13.8	11.8	9.9	8.2	6.6	5.1
		2	502	16.1	13.4	11.6	9.8	8.0	6.5	5.3
		3	509	14.6	13.2	11.3	9.6	7.9	6.4	5.0
		4*	389	26.0	9.3	8.2	7.0	5.9	4.5	2.8
		Adj	*500*	*16.7*	*13.7*	*11.8*	*9.9*	*8.2*	*6.5*	*5.3*
3	512	1	516	20.8	18.6	17.1	15.9	15.2	5.8	4.4
		2	516	20.2	18.1	16.6	15.3	14.4	5.9	4.5
		3	521	20.1	18.0	16.2	15.0	14.1	5.7	4.3
		4	407	15.0	13.9	12.4	11.3	10.7	4.3	3.2
		Adj	*500*	*19.5*	*17.5*	*15.9*	*14.7*	*13.9*	*5.6*	*4.2*

*Neglected in Analysis

Table 19 provides HWD deflection basins for Craters 4, 5, and 6, which are the three 8.5-ft by 8.5-ft craters that contained backfill. As observed in Table 18 (Craters 1, 2, and 3), results were not intuitive. Crater 4 (the weakest crater based on FF cap thickness and CBR values calculated from measured DCP results) had considerably lower deflections than Craters 5 or 6. Crater 4 had CBR values generally less than 5 percent in the backfill and somewhat lower subgrade CBR's than Craters 5 or 6, which had CBR values around an order of magnitude higher than Crater 4 and subgrade CBR values that were higher as well (around 30 percent in Craters 5 and 6). Crater 4 had CBR values around half that of Crater 5 or 6 in the top 6 in. of the subgrade. D_1 *Adj.* values ranged from 23.4 to 26.6, 34.4 to 34.5, and 32.1 to 45.0 mils in Craters 4, 5, and 6, respectively. There was a 5.5-mil separation between the highest D_1 *Adj.* value in Crater 4 and the lowest D_1 *Adj.* value in Crater 5 or 6. Craters 4 and 5 did not have considerable changes in deflection basins before and after trafficking, though Crater 6 had more than 10 mils of additional deflection after traffic. Crater 6 breaking down somewhat during traffic though Craters 4 and 5 did not is also counter-intuitive based on FF cap thicknesses, base-layer thicknesses, and as constructed CBR values. Crater 4's HWD measurements were the least intuitive values recorded and are not understood.

Table 20 and Table 21 provide HWD deflection basins for Craters 7 and 8, which were the only craters trafficked with C-17 loadings and, as such, these two craters were only compared to each other in the context of deflection measurements after trafficking. Crater 7 did not show much, if any, evidence of being damaged during trafficking relative to its pre-traffic levels (i.e., deflections were similar before and after trafficking), though as noted earlier, the amount of stiffness improvement over the duration of trafficking was not measured. Relative to Crater 3, Crater 7's pre-traffic deflections were modestly lower at 12.5 to 13.1 mils as compared to Crater 3's D_1 *Adj.* value of 16.7 mils.

Crater 8 did show some evidence of being damaged during trafficking, with D_1 *Adj.* values increasing from 7.4 to 11.4 mils during trafficking. This finding agrees with Crater 6 (same cross section, but loaded with F-15 traffic) where deflections increased 12.9 mils during trafficking. Prior to trafficking, Crater 8 had D_1 *Adj.* values between 28.7 to 34.7 mils, which agrees with Crater 6's pre-traffic D_1 *Adj.* value of 32.1 mils. Crater 8 also experienced around twice as much deflection as Crater 7 prior to trafficking, which is intuitive.

Table 19. HWD measurements in Craters 4, 5, and 6.

Crater	Passes	HWD Drop	Contact Stress (psi)	Deflection (mils)						
				D_1	D_2	D_3	D_4	D_5	D_6	D_7
4	0	1	494	29.9	26.3	22.6	18.7	15.6	12.8	10.2
		2	508	25.7	22.2	18.6	15.2	12.5	10.1	8.1
		3	506	25.2	21.6	18.1	14.7	12.0	9.8	7.8
		4	398	19.6	17.3	14.2	11.6	9.4	7.6	5.9
		Adj	*500*	*26.6*	*23.1*	*19.5*	*16.0*	*13.2*	*10.8*	*8.6*
4	512	1	490	23.4	20.2	16.9	13.8	11.4	9.5	8.0
		2	494	23.3	20.0	16.7	13.7	11.3	9.5	7.9
		3	502	22.9	19.3	16.1	13.3	11.0	9.2	7.7
		4	374	17.3	14.5	12.2	9.9	8.4	6.9	6.0
		Adj	*500*	*23.4*	*20.0*	*16.7*	*13.7*	*11.4*	*9.5*	*7.9*
5	0	1	463	33.4	29.4	24.2	19.5	15.7	12.4	9.8
		2	468	30.6	26.1	21.2	16.8	13.3	10.5	8.4
		3	470	31.2	26.1	21.2	16.6	13.1	10.4	8.3
		4	381	24.3	20.6	16.6	13.0	10.2	8.0	6.0
		Adj	*500*	*34.5*	*29.6*	*24.3*	*19.3*	*15.4*	*12.2*	*9.9*
5	512	1	470	32.5	28.5	24.0	19.8	16.4	13.4	11.1
		2	468	32.2	27.9	23.5	19.4	16.1	13.2	11.0
		3	468	31.9	27.9	23.3	19.1	15.8	13.0	10.8
		4	381	26.1	22.4	18.9	15.5	12.8	10.6	8.5
		Adj	*500*	*34.4*	*30.1*	*25.3*	*20.8*	*17.2*	*14.1*	*11.9*
6	0	1	484	32.3	28.1	23.7	19.1	15.1	11.5	8.5
		2	489	29.2	24.6	20.5	16.3	12.7	9.7	7.2
		3*	478	62.1	23.5	19.3	15.2	11.9	9.0	6.7
		4*	347	94.0	16.6	14.0	11.0	7.5	6.3	4.3
		Adj	*500*	*32.1*	*27.7*	*23.4*	*19.0*	*15.2*	*11.9*	*9.2*
6	512	1	460	42.7	39.1	32.8	26.9	21.3	15.8	11.7
		2	465	42.0	36.4	31.4	25.4	19.9	15.3	11.1
		3*	447	114.7	34.9	28.8	23.3	18.4	13.8	10.1
		4*	352	129.0	29.4	24.6	20.0	15.9	12.2	8.8
		Adj	*500*	*45.0*	*40.4*	*34.7*	*28.8*	*23.2*	*18.2*	*14.0*

*Neglected in Analysis. Crater 6 Adj. values estimated based on Crater 5 stress to deflection relationship.

Table 20. HWD measurements of Crater 7.

Crater	Station	Passes	HWD Drop	Contact Stress (psi)	Deflection (mils)						
					D_1	D_2	D_3	D_4	D_5	D_6	D_7
7	A	0	1	516	14.0	10.5	9.2	8.1	7.2	6.0	5.1
			2	516	13.1	9.2	8.1	7.1	6.2	5.2	4.6
			3*	471	74.0	8.0	7.1	6.1	5.5	4.5	3.7
			4*	354	52.4	6.4	5.6	5.1	4.2	4.2	4.1
			Adj	*500*	*13.1*	*9.4*	*8.2*	*7.1*	*6.2*	*5.1*	*4.4*
7	A	504	1	519	15.9	13.8	12.8	11.7	10.9	10.5	9.7
			2	517	15.9	13.8	12.8	11.4	10.6	10.5	9.4
			3	512	15.6	12.9	12.0	11.0	10.3	9.7	9.0
			4*	386	47.2	10.1	9.4	8.6	7.7	7.6	6.6
			Adj	*500*	*15.3*	*13.2*	*12.2*	*11.0*	*10.2*	*10.0*	*9.0*
7	B	0	1	504	13.1	10.8	9.7	8.7	7.8	6.8	6.1
			2	503	12.4	10.2	9.1	8.0	7.2	6.3	5.5
			3	505	12.4	10.4	9.0	8.2	7.2	6.3	5.6
			4	409	9.9	7.8	7.0	6.2	5.5	4.9	4.3
			Adj	*500*	*12.6*	*10.3*	*9.2*	*8.2*	*7.3*	*6.4*	*5.7*
7	B	504	1	512	14.0	11.1	9.6	8.2	7.0	5.7	4.6
			2	513	13.5	10.7	9.2	7.8	6.8	5.4	4.4
			3	523	13.6	10.6	9.0	7.7	6.7	5.4	4.4
			4*	417	16.1	7.7	6.8	5.6	5.2	3.8	3.2
			Adj	*500*	*13.0*	*10.3*	*8.8*	*7.5*	*6.4*	*5.1*	*4.0*
7	C	0	1	499	12.8	9.9	8.5	7.3	6.3	5.2	4.3
			2	499	12.3	9.2	8.1	6.9	5.9	4.9	4.1
			3	498	12.1	9.1	7.9	6.8	5.9	4.8	4.0
			4	400	9.7	6.9	6.1	5.2	4.5	3.7	3.1
			Adj	*500*	*12.5*	*9.4*	*8.2*	*7.0*	*6.0*	*5.0*	*4.1*
7	C	504	1	533	14.5	13.1	12.9	12.9	8.8	5.0	4.2
			2	534	14.0	12.3	11.9	11.9	8.4	5.2	4.3
			3*	529	23.2	11.9	11.5	11.4	8.1	5.2	4.2
			4*	382	65.5	8.9	8.7	9.4	6.1	3.3	3.9
			Adj	*500*	*13.2*	*11.5*	*11.5*	*11.5*	*7.7*	*4.5*	*3.8*

*Neglected in Analysis. Station B, 0 passes was used as a reference for all groups with an (*).

Table 21. HWD measurements in Crater 8.

Crater	Station	Passes	HWD Drop	Contact Stress (psi)	Deflection (mils)						
					D_1	D_2	D_3	D_4	D_5	D_6	D_7
8	A	0	1*	461	68.7	22.1	17.8	13.5	10.3	7.3	5.5
			2*	472	46.7	25.4	19.9	15.0	11.1	8.0	5.8
			3*	482	46.3	26.0	20.4	15.3	11.3	8.2	5.9
			4*	395	36.0	20.6	16.2	12.2	8.9	6.4	4.7
			Adj	500	---	---	---	---	---	---	---
8	A	504	1	480	38.4	34.5	22.0	13.9	10.8	8.0	5.9
			2	486	36.3	33.7	20.6	13.7	10.6	7.8	5.9
			3	482	35.5	34.2	19.1	13.4	10.4	7.9	6.2
			4	376	28.2	24.8	14.9	10.4	8.2	6.9	5.0
			Adj	500	38.1	35.6	21.5	14.2	10.9	8.1	6.1
8	B	0	1	482	28.5	23.8	19.1	14.4	10.7	8.0	6.5
			2	481	26.7	21.5	16.8	12.4	9.1	7.1	5.9
			3	480	26.8	21.4	16.7	12.4	8.9	7.0	5.8
			4	388	20.8	16.6	12.9	9.5	6.9	5.4	4.5
			Adj	500	28.7	23.4	18.5	13.8	10.1	7.7	6.4
8	B	504	1	470	40.7	33.1	24.9	17.3	11.7	7.7	5.6
			2	477	36.6	30.3	23.2	16.4	11.3	7.9	5.7
			3	478	36.9	30.5	22.9	16.2	11.1	8.0	5.8
			4	381	29.7	24.4	18.5	13.0	8.7	6.1	4.5
			Adj	500	40.1	33.0	24.9	17.6	12.0	8.3	6.0
8	C	0	1	471	34.2	27.0	20.7	15.6	11.7	8.6	6.4
			2	475	31.9	24.4	18.6	13.9	10.4	7.8	5.9
			3	478	31.3	24.8	18.6	13.8	10.3	7.6	5.8
			4	391	24.6	18.8	14.2	10.4	7.9	5.8	4.5
			Adj	500	34.7	27.3	20.8	15.6	11.6	8.6	6.5
8	C	504	1	464	40.5	31.9	25.2	16.6	11.0	7.1	10.8
			2	468	37.6	29.7	23.3	15.4	10.4	6.8	5.2
			3*	474	71.5	29.4	23.1	15.2	10.3	6.8	5.1
			4*	386	45.7	23.2	18.1	11.9	8.7	5.9	4.4
			Adj	500	42.1	33.8	27.3	19.0	13.7	10.0	11.0

*Neglected in Analysis. Station B, 504 passes was used as a reference for Station C, 504 passes.

Overall, there were not many definitive findings from HWD testing. In many respects, HWD testing of flowable fill cap materials was an exploratory effort; a small percentage of the overall budget was devoted to HWD testing. Perhaps one of the most useful manners in which to use the HWD data collected is to plan for more detailed experiments with flowable fill cap materials. Two items are recommended for future assessments of flowable fill craters based on HWD testing. The first is to more comprehensively document flowable fill cap materials as placed within individual craters. It is suspected that at least some of the non-intuitive behaviors may be related to unknown differences between the flowable fill cap properties. One possible explanation for some of the non-intuitive HWD deflection basin results between craters could be differences in properties in the flowable fill caps themselves (gate settings in particular). Detailed property characterization for flowable fill capping material when placed at full-scale has not been completed. Detailed understanding of how, for example, gate settings affect in-place properties is needed to make a more detailed assessment of flowable fill HWD data. The second recommendation is to pour individual craters (or parts of craters) and test their response over time with the HWD absent traffic to help decouple strength gain with time and trafficking effects.

Figure 52 and Figure 53 take a global view of seven of the eight craters constructed by plotting deflection basin envelopes for full depth flowable fill (Craters 1, 2, 3, and 7), and craters that are approximately half crushed stone backfill and half flowable fill capping (Craters 5, 6, and 8). When the overall perspective of these experiments is of primary emphasis (as opposed to specific comparisons between sections) and the unexplained HWD measurements in Crater 4 are neglected, the Figure 52 and Figure 53 results provide a reasonable overall picture of response between backfilled and non-backfilled craters surfaced with flowable fill. Craters absent backfill (Figure 52) are much less affected by traffic, have much lower deflections, and have flatter deflection basins (implying the crater is moving somewhat as a unit into the underlying subgrade). The overall trends depicted in Figure 52 and Figure 53 are much more intuitive and are recommended to be the main take-away from the HWD experiments performed to date. As mentioned earlier, additional data would be needed for a more sophisticated decoupling of behavior during early age trafficking of flowable fill.

Figure 52. HWD deflection basins adjusted to 500 psi stress for full-depth flowable fill craters (20 to 24 in.).

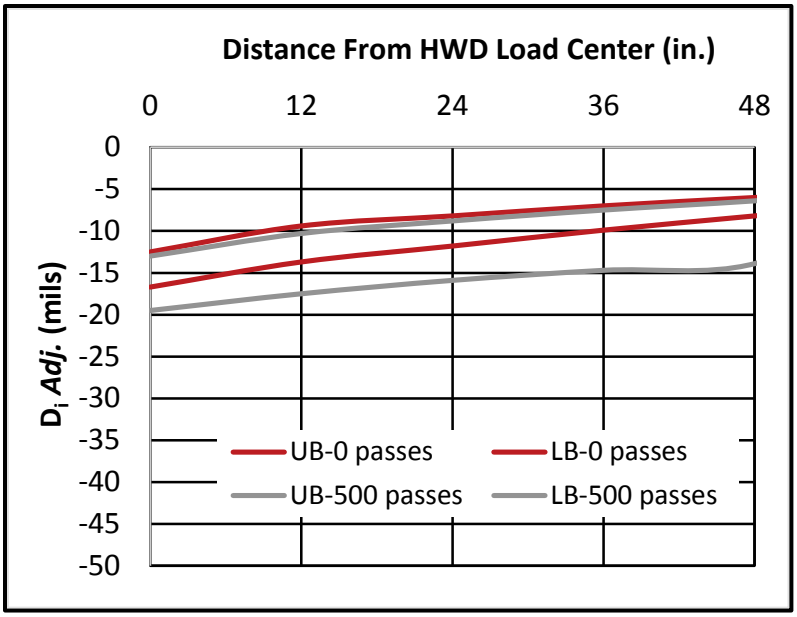

Figure 53. HWD deflection basins adjusted to 500 psi stress for 10 to 12 in. of crushed stone backfill with 12-in. flowable fill cap.

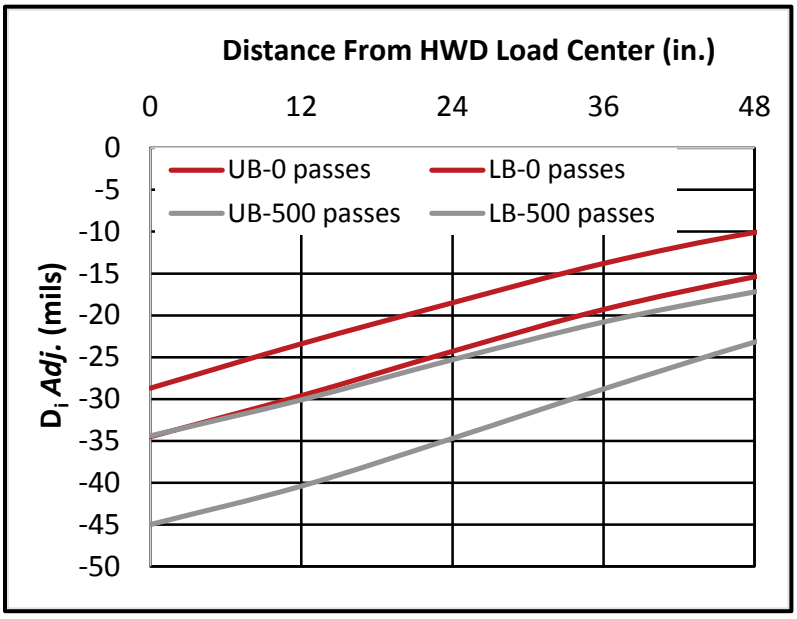

4.6 Core sample test results

Three core samples were obtained from Craters 4 through 8 to obtain thickness measurement and compressive strength testing at 28 days; the results are displayed in Table 22. The cores were taken from random locations within the crater to obtain an average compressive strength for each crater. The compressive strengths for Craters 4, 5, and 6 were

considerably higher than Craters 7 and 8. The higher compressive strength was expected since a much more fluid consistency of flowable fill was used for the larger craters than the smaller craters, resulting in a higher w/c ratio as discussed in Section 3.3.

Table 22. Core sample lengths and compressive strengths.

Crater	Length (in.)	Avg Core Length (in.)	Table 13 Surveyed Layer Thicknesses (in.)	28-day Compressive Strength (psi)	Avg. 28-day Compressive Strength (psi)
4	12.00	11.9	11.9	2,790	2,337
	11.75			2,120	
	12.00			2,100	
5	11.50	11.4	10.7	2,270	2,140
	11.25			1,980	
	11.50			2,170	
6	12.25	12.3	12.1	2,010	2,007
	12.25			1,960	
	12.50			2,050	
7	N/A	N/A	24.3	1,630	1,477
	N/A			1,610	
	N/A			1,190	
8	13.25	13.0	10.9	950	1,273
	12.25			1,360	
	13.50			1,510	

The measured core thicknesses for Crater 4 were very close to the target of 12 in., while the measured core thicknesses for Crater 5 averaged 0.6 in. less than the target of 12 in. The thicknesses obtained for Crater 6 were within 0.3 in. of the 12-in. target. The target thickness for Crater 8 was 12 in., and the average core thickness was 1 in. thicker than the target. Although many of the thickness measurements obtained from core samples are thicker than the target, the survey results discussed in Section 4.4.5 should be considered a more accurate overall thickness measurement, and those results indicate that target thicknesses were reasonably achieved in general. These survey results are repeated in Table 22.

5 Conclusions and Recommendations

The main objective of the flowable fill surface performance testing was to determine if flowable fill placed using the volumetric mixer (wet method) can be used as a surface capping material over various base courses or the natural subgrade. Once this objective was met, recommendations were needed concerning the expected number of aircraft passes that could be sustained. The following sections provide the conclusions developed from testing along with the accompanying recommendations.

5.1 Conclusions

- After approximately 2 hr of cure time, crater repairs capped with rapid-setting flowable fill failed after approximately 500 simulated F-15 (small craters) or C-17 (large craters) aircraft passes, meeting the requirement for an expedient crater repair (100 passes).
- Placement and finishing times for rapid-setting flowable fill would likely be similar or less than that of rapid-setting concrete since the rapid-setting flowable fill is more workable.
- The mode of failure observed did not appear to be structural in nature. High-severity spalling around the edges in the direction of traffic was the typical mode of failure exhibited, which is consistent with previous ADR research on craters capped with rapid-setting concrete.
- Small changes to the gate setting on the ADR simplified volumetric mixer can considerably increase the workability of the flowable fill during placement. However, increasing the workability will likely decrease the UCS and could create small areas of weaker material throughout the repair.
- Overall, there were not many definitive conclusions from HWD testing when the data was used to compare results between crater repairs and before and after traffic. HWD data did clearly show craters with 20 to 24 in. of flowable fill outperforming 12 in. of flowable fill with 10 to 12 in. of crushed stone backfill. Visual observations under traffic and survey data were much more informative and conclusive when considering the overall objective of the testing described in this report.

5.2 Recommendations

- Rapid-setting flowable fill is recommended for consideration to use as a surface capping material for crater repairs that are expected to receive 500 or fewer passes during a set period of aircraft operations. Frequent sweeping of the area would likely be required to remove trafficking debris.
- When placing rapid-setting flowable fill using the ADR simplified volumetric mixer in moderately high ambient temperatures (approximately 85°F), a gate setting of 7 is recommended to maximize the durability of small crater repairs. A gate setting of 5.5 to 6 is recommended for large craters to increase workability. A higher gate setting may be used in colder ambient temperatures since the set time would likely be increased.
- Future testing is recommended using rapid-setting flowable fill as a capping material at additional thicknesses and base courses to establish design curves that correspond with those developed by Priddy et al. (2016).
- It is recommended that rapid-setting flowable fill be considered for inclusion as a capping material in future live aircraft certification tests.
- If baseline HWD data is desired to use for estimation of in-situ modulus values, a more comprehensive documentation of flowable fill cap materials as placed within individual craters is needed. Also, it is recommended to place individual craters and test their response over time with the HWD absent traffic to document strength gain with time.

References

Air Force Civil Engineer Center. 2014. *Interim tactics, techniques, and procedures: Airfield Damage Repair (ADR) interim process for base recovery after attack*. Tyndall AFB, FL: AFCEC.

American Society for Testing and Materials (ASTM). 2004. Standard test methods for density of soil and soil-aggregate in place by nuclear methods (shallow depth). C2922. In *Annual book of ASTM standards*. West Conshohocken, PA: American Society for Testing Materials.

_____. 2004. Standard test method for water content of soil and rock in place by nuclear methods (shallow depth). D3017. In *Annual book of ASTM standards*. West Conshohocken, PA: American Society for Testing Materials.

_____. 2004. Standard test method for flow consistency of controlled low strength material (CLSM). D6103. In *Annual book of ASTM standards*. West Conshohocken, PA: American Society for Testing Materials.

_____. 2009. Standard test method for use of the dynamic cone penetrometer in shallow pavement applications. D6951. In *Annual book of ASTM standards*. West Conshohocken, PA: American Society for Testing Materials.

_____. 2011. Standard practice for classification of soils for engineering purposes (Unified Soil Classification System). D2487. In *Annual book of ASTM standards*. West Conshohocken, PA: American Society for Testing Materials.

Bell, H. P., L. Edwards, W. D. Carruth, J. S. Tingle, and J. R. Griffin. 2013. *Wet weather crater repair testing at silver flag exercise site, Tyndall Air Force Base, Florida*. ERDC/GSL TR-13-42. Vicksburg, MS: U.S. Army Engineer Research and Development Center.

Carruth, W. D., L. Edwards, H. P. Bell, J. S. Tingle, J. R. Griffin, and C. A. Rutland. 2015. *Large crater repair at Silver Flag exercise site, Tyndall Air Force Base, Florida*. ERDC/GSL TR 15-27. Vicksburg, MS: U.S. Army Engineer Research and Development Center.

Edwards, L., H. P. Bell, W. D. Carruth, J. R. Griffin, and J. S. Tingle. 2013. *Cold weather crater repair testing at Malmstrom Air Force Base, Montana*. ERDC/GSL TR-13-32. Vicksburg, MS: U.S. Army Engineer Research and Development Center.

Lovingood, D., Eichler, J., Griffith, K., and Henley, M. 2015. *Effects of non-potable water sources on rapid-setting cementitious materials used in airfield damage repair*. Report No. AFCEC-CX-TY-TP-2016-0001. Tyndall Air Force Base, FL: Air Force Civil Engineer Center.

Priddy, L. P., H. P. Bell, L. Edwards, W. D. Carruth, and J. F. Rowland. 2016. *Evaluation of the structural performance of Rapid Set Concrete Mix®*. ERDC/GSL TR-16-20. Vicksburg, MS: U.S. Army Engineer Research and Development Center.

Priddy, L. P., J. S. Tingle, M. C. Edwards, J. R. Griffin, and T. J. McCaffrey. 2013. *Critical Runway AssessmenT and Repair (CRATR) technology demonstration: Limited Operational Utility Assessment 2 (LOUA2), Tyndall Air Force Base, Florida*. ERDC/GSL TR-13-39. Vicksburg, MS: U.S. Army Engineer Research and Development Center.

REPORT DOCUMENTATION PAGE

Form Approved
OMB No. 0704-0188

1. REPORT DATE *(DD-MM-YYYY)*	2. REPORT TYPE	3. DATES COVERED *(From - To)*
November 2016	Final	

4. TITLE AND SUBTITLE

Evaluation of Flowable Fill Surface Performance

5a. CONTRACT NUMBER

5b. GRANT NUMBER

5c. PROGRAM ELEMENT NUMBER

6. AUTHOR(S)

William D. Carruth and Dr. Isaac L. Howard

5d. PROJECT NUMBER
333159

5e. TASK NUMBER

5f. WORK UNIT NUMBER
18F04H

7. PERFORMING ORGANIZATION NAME(S) AND ADDRESS(ES)

Geotechnical and Structures Laboratory
U.S. Army Engineer Research and Development Center
3909 Halls Ferry Road
Vicksburg, MS 39180-6199

8. PERFORMING ORGANIZATION REPORT NUMBER

ERDC/GSL TR-16-33

9. SPONSORING / MONITORING AGENCY NAME(S) AND ADDRESS(ES)

Headquarters, Air Force Civil Engineer Center
Tyndall AFB, FL 32403-5319

10. SPONSOR/MONITOR'S ACRONYM(S)

AFCEC

11. SPONSOR/MONITOR'S REPORT NUMBER(S)

12. DISTRIBUTION / AVAILABILITY STATEMENT

Approved for public release; distribution is unlimited.

13. SUPPLEMENTARY NOTES

14. ABSTRACT

In 2004, legacy ADR systems were found to be inadequate for supporting runway operations of large military aircraft. The inability to effectively operate both fighter and heavy cargo aircraft on the same repaired runway after an attack poses significant operational challenges. The U.S. Air Force Air Combat Command began the Airfield Damage Repair (ADR) Modernization Program to develop technologies to address operational limitations of current ADR equipment, materials, and tactics. The objective of the program was to modernize the Air Force's ADR capability through development of new solutions suitable for both fighter and cargo aircraft and scalable to the threat or damage. Scalable ADR solutions improve minimum operating strip (MOS) decision making options. Technical solutions were successfully demonstrated as a part of the Critical Runway AssessmenT and Repair (CRATR) Joint Capabilities Technology Demonstration (JCTD) Program. One of the solutions successfully demonstrated was use of rapid-setting flowable fill backfill. This report describes testing of rapid-setting flowable fill material as a surface capping material for expedient crater repairs at the Silver Flag Exercise Site on Tyndall Air Force Base, Florida. Repairs were capped with rapid-setting flowable fill over varying types and thicknesses of backfill layers. Smaller-sized repairs were loaded with a load cart simulating F-15 aircraft traffic, while larger repairs were trafficked with simulated C-17 traffic. All repairs withstood more than 500 simulated aircraft passes before reaching failure.

15. SUBJECT TERMS

Airfield Damage Repair
Flowable fill
Cratering
Rapid-setting
Crater repair
Base recovery
Runways (Aeronautics) – Maintenance and repair
Controlled low-strength materials
Fills (Earthwork)
Pavements, Concrete-Cracking

16. SECURITY CLASSIFICATION OF:			17. LIMITATION OF ABSTRACT	18. NUMBER OF PAGES	19a. NAME OF RESPONSIBLE PERSON
a. REPORT	b. ABSTRACT	c. THIS PAGE			19b. TELEPHONE NUMBER *(include area code)*
Unclassified	Unclassified	Unclassified		75	